

Decitabine potentiates efficacy of doxorubicin in a preclinical trastuzumab-resistant HER2-positive breast cancer models

Verona Buocikova^a, Eleonora Marta Longhin^b, Eleftherios Pilalis^{c,d}, Chara Mastrokalou^d, Svetlana Miklikova^a, Marina Cihova^a, Alexandra Poturnayova^e, Katarina Mackova^e, Andrea Babelova^a, Lenka Trnkova^a, Naouale El Yamani^b, Congying Zheng^f, Ivan Rios-Mondragon^g, Martina Labudova^h, Lucia Csaderova^h, Kristina Mikus Kuracinovaⁱ, Peter Makovicky^a, Lucia Kucerova^a, Miroslava Matuskova^a, Mihaela Roxana Cimpan^g, Maria Dusinska^b, Pavel Babalⁱ, Aristotelis Chatziioannou^{c,d}, Alena Gabelova^a, Elise Rundén-Pran^b, Bozena Smolkova^{a,*}

^a Cancer Research Institute, Biomedical Research Center of the Slovak Academy of Sciences, Dubravská cesta 9, 845 05 Bratislava, Slovakia

^b Health Effects Laboratory, NILU-Norwegian Institute for Air Research, 2007 Kjeller, Norway

^c e-NIOS Applications P.C., Alexandrou Pantou 25, Kallithea 17671, Athens, Greece

^d Center of Systems Biology, Biomedical Research Foundation of the Academy of Athens, Greece

^e Institute of Molecular Physiology and Genetics, Centre of Biosciences, Slovak Academy of Sciences, Dubravská cesta 9, 845 05 Bratislava, Slovakia

^f Norgenotech AS, Ullernchassern, 64/66 Oslo, Norway

^g Department of Clinical Dentistry, University of Bergen, Aarstadveien 19, 5009 Bergen, Norway

^h Institute of Virology, Biomedical Research Center of the Slovak Academy of Sciences, Dubravská cesta 9, 845 05 Bratislava, Slovakia

ⁱ Department of Pathology, Faculty of Medicine, Comenius University in Bratislava, Sasinkova 4, 811 08 Bratislava, Slovakia

ARTICLE INFO

Keywords:

Breast cancer
Epigenetic drugs
Combination therapy
Decitabine
Doxorubicin
DNA methylation

ABSTRACT

Acquired drug resistance and metastasis in breast cancer (BC) are coupled with epigenetic deregulation of gene expression. Epigenetic drugs, aiming to reverse these aberrant transcriptional patterns and sensitize cancer cells to other therapies, provide a new treatment strategy for drug-resistant tumors. Here we investigated the ability of DNA methyltransferase (DNMT) inhibitor decitabine (DAC) to increase the sensitivity of BC cells to anthracycline antibiotic doxorubicin (DOX). Three cell lines representing different molecular BC subtypes, JIMT-1, MDA-MB-231 and T-47D, were used to evaluate the synergy of sequential DAC + DOX treatment *in vitro*. The cytotoxicity, genotoxicity, apoptosis, and migration capacity were tested in 2D and 3D cultures. Moreover, genome-wide DNA methylation and transcriptomic analyses were employed to understand the differences underlying DAC responsiveness. The ability of DAC to sensitize trastuzumab-resistant HER2-positive JIMT-1 cells to DOX was examined *in vivo* in an orthotopic xenograft mouse model. DAC and DOX synergistic effect was identified in all tested cell lines, with JIMT-1 cells being most sensitive to DAC. Based on the whole-genome data, we assume that the aggressive behavior of JIMT-1 cells can be related to the enrichment of epithelial-to-mesenchymal transition and stemness-associated pathways in this cell line. The four-week DAC + DOX sequential administration significantly reduced the tumor growth, DNMT1 expression, and global DNA methylation in xenograft tissues. The efficacy of combination therapy was comparable to effect of pegylated liposomal DOX, used exclusively for the treatment of metastatic BC. This work demonstrates the potential of epigenetic drugs to modulate cancer cells' sensitivity to other forms of anticancer therapy.

1. Introduction

Breast cancer (BC) remains one of the most common cancer types and

a leading cause of cancer-related deaths among women worldwide [1]. Although innovative medical modalities and multidisciplinary approaches have contributed significantly to improved effectiveness of modern therapeutic regimens, the gradual development of drug

* Corresponding author.

E-mail address: bozena.smolkova@savba.sk (B. Smolkova).

<https://doi.org/10.1016/j.bioph.2022.112662>

Received 29 November 2021; Received in revised form 14 January 2022; Accepted 19 January 2022

Available online 25 January 2022

0753-3322/© 2022 The Authors.

Published by Elsevier Masson SAS. This is an open access article under the CC BY-NC-ND license

(<http://creativecommons.org/licenses/by-nc-nd/4.0/>).

resistance remains a serious clinical problem [2,3]. HER2-positive BC is a hormone-receptor negative, HER2-enriched molecular subtype, with

trapped in the process, leading to depletion of DNMT1 from the cells and passive demethylation. DAC also indirectly induces changes in gene

Nomenclature			
AB	AlamarBlue	Fa	Fraction affected
ANOVA	Analysis of variance	FC	Fold change
BC	Breast cancer	FDA	Food and Drug Administration
bw	Bodyweight	FDR	False Discovery Rate
CI	Combination index	Fpg	Formamidopyrimidine DNA glycosylase
CFE	Colony forming efficiency	HE	Hematoxylin and eosin
CX	Caelyx®	HER2	Human epidermal growth factor receptor 2
DAC	Decitabine	i.p.	Intraperitoneal injection
DDR	DNA damage response	LINE-1	Long interspersed nucleotide element 1
DNMT	DNA methyltransferase	NC	Negative control
DNMTi	DNA methyltransferase inhibitors	NST	No special type
DOX	Doxorubicin	PC	Positive control
ECM	Extracellular matrix	PR	Progesterone receptor
Epi-drugs	Epigenetic drugs	qPCR	Quantitative real-time PCR
ER	Estrogen receptor	SB	Strand breaks
		SC	Solvent control
		SEM	Standard error of mean

faster growth and worse prognosis than luminal cancer. Nevertheless, it is often successfully treated with monoclonal antibodies (trastuzumab - Herceptin®, pertuzumab - Perjeta®) targeting the *ERBB2* (Erb-B2 Receptor Tyrosine Kinase 2) gene product, commonly referred to as HER2. Additionally, there are two other categories of FDA-approved anti-HER2 drugs currently used in HER2-positive BC patients, such as trastuzumab-drug conjugates (trastuzumab emtansine - Kadcyła®, trastuzumab deruxtecan - Enhertu®, and pertuzumab trastuzumab hyaluronidase - Phesgo®) and small-molecule tyrosine kinase inhibitors (neratinib - Nerlynx®, lapatinib - Tykerb®, and tucatinib - Tukysa®) [4]. However, acquired resistance to these drugs strongly limits therapeutic options for non-responsive patients. Nowadays, epigenetic dysregulation has been recognized as a critical factor influencing drug resistance and metastasis. Accordingly, epigenetic silencing of the *ERBB2* is considered the primary mechanism of HER2-positive BC resistance to trastuzumab [5–7].

Indeed, in preclinical models, epigenetic drugs (epi-drugs) have been shown to sensitize resistant cancer cells to chemotherapy and thus increase the efficacy of other therapeutic approaches [8]. Despite these promising findings, the application of epi-drugs in clinical settings is not straightforward. Except for tazemetostat (Tazverik®), a selective histone-lysine N-methyltransferase EZH2 inhibitor approved by the FDA in 2020 to treat metastatic or locally advanced epithelioid sarcoma, no other epi-drug has been approved by now for solid tumors.

Overall, the cancer genome is hypomethylated, while hypermethylation is mainly found in gene promoter regions containing CpG rich islands [9]. The hypomethylation agent decitabine (DAC), approved for treating myelodysplastic syndrome and acute myeloid leukemia, is a deoxycytidine analog typically used to reactivate gene expression silenced by promoter methylation [10]. In solid tumors, DAC was studied by default as a cytotoxic agent using high micromolar concentrations. It induced DNA-adduct formation that impeded DNA polymerase functions, leading to cell death and activation of DNA damage response (DDR) and DNA repair pathways [11,12]. The success of this approach for solid tumor treatment has been limited in clinical trials due to unwanted high toxicity. At nanomolar concentrations, DAC does not hamper DNA synthesis, and its hypomethylating effect is more pronounced. DNA methyltransferases (DNMTs) are responsible for maintaining established methylation patterns (DNMT1) and mediating *de novo* DNA methylation (DNMT3A, DNMT3B) [11]. After DAC incorporation into DNA, DNMT1 initiates a methyltransferase reaction but is

expression without affecting DNA methylation of the target gene. These indirect effects are mediated via demethylation of upstream genes, regulatory elements, secondary responses to DNA damage, and repair mechanisms caused by DAC toxicity or changes in histone modifications [12]. Interestingly, Tsai et al. have shown that exposure of epithelial tumor cells to DAC at nanomolar concentrations produced an antitumor "memory" response, mediated by a sustained decrease in genome-wide promoter DNA methylation and gene re-expression in key cellular regulatory pathways [13]. DAC in combination with chemotherapy has been used in preclinical models for the treatment of the luminal A and triple-negative BC subtypes. The tumor cells turned out to be more sensitive to combination therapy than conventional chemotherapy [14–17]. Trastuzumab-resistant HER2-positive BC has not yet been studied in this context.

The anthracycline antibiotic doxorubicin (DOX) is an anticancer drug commonly used in BC treatment, whose antitumor activity is mediated by inhibition of topoisomerase II, hampering DNA replication due to DNA intercalation and DNA double-strand breaks induction. By DNA intercalation, DOX can cause histone eviction from transcriptionally active chromatin, resulting in epigenomic and transcriptomic changes, DDR signaling activation, and apoptosis [18]. Although the combination of DOX with the monoclonal antibody trastuzumab (Herceptin®) enhanced antitumor activity and overall response rate in HER2-positive BC patients, unacceptably high rates of cardiotoxicity limit their co-administration in clinical settings [19,20]. Liposome-encapsulated nanoforms of DOX, as the pegylated alternatives Doxil®, Caelyx® (CX), or non-pegylated liposomal DOX (Myocet®), are clinically used for the treatment of metastatic BC. They might serve as an alternative to free DOX in combination therapies due to their decreased toxicity.

Here, we investigated the inhibitory effect of low-dose DAC combined with standard chemotherapy *in vitro* on BC cell lines JIMT-1, MDA-MB-231, and T-47D, representing different clinical subtypes. In addition, an integrative approach with genome-wide DNA methylation (Infinium Methylation EPIC array) and a transcriptomic analysis (RNA-Seq) was applied to shed light on differences in DAC responsiveness. Furthermore, the trastuzumab-resistant HER2-positive orthotopic mouse model was developed to assess the efficacy of combination therapy. Apart from tumor growth and histopathological examination, the functional effect on DNMTs expression and DNA methylation was evaluated. The efficacy of DAC + DOX treatment was compared with

that of liposome-encapsulated nanoform of DOX - Caelyx®. Our study aimed to test the hypothesis that DAC at low concentrations is able to increase the sensitivity of BC cells to chemotherapy.

2. Materials and methods

2.1. Cell cultures

Three human epithelial BC cell lines were used: JIMT-1 (DSMZ no.: ACC 589) high-grade invasive ductal carcinoma cells (estrogen receptor (ER)-; progesterone receptor (PR)-; HER2+); MDA-MB-231 (ATCC® Number: HTB-26™) triple-negative cells (ER-, PR-, HER2-), and T-47D (ATCC® HTB-133™) luminal A subtype cells (ER+, PR+/-, and HER2-) isolated from pleural effusion of mammary gland adenocarcinoma patients. Cell lines were authenticated in July 2018 by the short tandem repeat DNA profiling. All cells were maintained in high-glucose (4.5 g/l) Dulbecco's modified Eagle medium (DMEM, PAA Laboratories GmbH, Pasching, Austria) supplemented with 10% fetal bovine serum (FBS, Biochrom AG, Berlin, Germany), 2 mM glutamine (PAA Laboratories GmbH), and 10 µg/ml gentamicin (Sandoz, Nürnberg, Germany). Cells were cultivated at 37 °C in a humidified atmosphere and 5% CO₂.

3D multicellular aggregates (spheroids) were prepared by seeding cells into 96-well round-bottom ultra-low attachment plates (Corning 7007, Corning Inc., Corning, NY, USA) at a density of 4×10^3 cells/well in 100 µl of ice-cold complete culture medium supplemented with extracellular matrix (ECM) Gel from Engelbreth-Holm-Swarm murine sarcoma (Sigma-Aldrich, Taufkirchen, Germany). The ECM, thawed and kept on ice, was added at a final concentration of 2% for JIMT-1 and MDA-MB-231, 0.5% for T-47D single-cell suspensions. Immediately after seeding, the cells were centrifuged at 1000 rpm for 10 min.

2.2. Cell exposure

For 2D cultures, the cells were seeded into 96-well plates at a density of 2.8×10^3 cells/well for JIMT-1, 1.1×10^3 cells/well for MDA-MB-231, and 3.5×10^3 cells/well for T-47D. The next day, cells were treated with different concentrations of DAC (MedChem Express, Shanghai, China) (0.0002–4 µg/ml) for 24 h or 6 days, DOX (Sigma-Aldrich, Taufkirchen, Germany) or CX (Janssen-Cilag NV, Beerse, Belgium) (0.002–0.200 µg/ml) for 5 days after which the effect of monotherapy was evaluated. CX was used to compare its efficacy with free DOX. In case of the combined treatment, cells were pre-treated with DAC for 24 h in a complete medium, followed by adding DOX for 5-day incubation. The cell confluency was analyzed using IncuCyte ZOOM™ Live-Cell Imaging System (Essen BioScience, Hertfordshire, UK) and IncuCyte ZOOM 2016A software as recommended by the manufacturer.

Cells in 3D cultures were allowed to form spheroids for three days before 6-day exposure to DAC (0.01–12 µg/ml) or 5-day exposure to DOX (0.01–1.00 µg/ml), simulating monotherapy. The sequential combined treatment was performed in the same way as for the 2D cell cultures. Unexposed cells were run in parallel as a negative control (NC). Positive control (PC) was Chlorpromazine (50 µM) and solvent controls (SCs) were DMSO for DAC (max. dose for 2D cultures: 0.0075%; 3D cultures: 0.075%) and sterile H₂O for DOX (max. dose for 2D cultures: 0.0002%; 3D cultures: 0.0005%).

2.3. Cell viability analyses

2.3.1. CellTiter-Glo® Luminescent Cell Viability Assay

Cell viability was determined by CellTiter-Glo® Luminescent Cell Viability Assay (Promega Corporation, Madison, WI) and CellTiter-Glo® 3D Cell Viability Assay (Promega Corporation, Madison, WI) and analyzed by GloMax® Discover Microplate Reader (Promega Corporation, Madison, WI). It was determined as the luminescence intensity relative to untreated control cells (set to 100%). The results are

presented as mean ± standard error of mean (SEM) from three independent experiments in quadruplicates. The IC₅₀ values and the combined effect of drugs were calculated according to Chou using CalcuSyn software (Biosoft, Cambridge, UK) [21]. Briefly, a combination index (CI) was calculated for every affected fraction (Fa, the proportion of dead cells): CI < 1 represents synergism, CI = 1 represents additivity, CI > 1 indicates antagonism.

2.3.2. The AlamarBlue assay

The AlamarBlue (AB) assay was integrated into the experimental procedure of the comet assay and was performed in the same experiment with the comet assay under the same conditions and exposure time [22]. The cells were seeded and exposed as described above. At least three independent experiments were performed for each cellular model, with samples run in duplicate within each experiment. After the exposure, the cells were incubated for 3 h in a fresh culture medium supplemented with 10% AB staining solution, and the fluorescence was measured on a microplate reader (FLUOstar OPTIMA, excitation 530 nm, emission 590 nm). Cell viability was quantified by calculating the fluorescence intensity relative to the NC (set to 100%) after subtracting the blank value (well with only medium and AB solution).

2.3.3. Colony forming efficiency assay

The colony forming efficiency (CFE) assay was used as published previously [23]. Briefly, approximately 30 cells/well were seeded in 12-well plates. The cells were allowed to settle for at least one hour before exposure. Then, the cells were exposed for 10 days to increasing DAC concentrations in the single treatment approach. For the combined treatment, the cells were pre-treated with DAC for 24 h, DOX was added for 5 days. Six replicate wells were used for the same sample. The medium was replaced at the end of exposure, and cells were further incubated for three weeks to form colonies. The cells were then stained with 1% methylene blue for approximately 1 h, and the number of colonies was counted manually. The results were normalized to the unexposed control (set to 100% colony forming efficiency).

2.4. Spheroid Migration Assay

Multicellular spheroids of 4×10^3 cells/well were prepared in six parallels per sample. Three days after seeding, JIMT-1, MDA-MB-231, and T-47D spheroids were pre-treated with 3.4 ng/ml, 2300 ng/ml, and 690 ng/ml DAC, respectively, for 24 h. Thereafter, DOX was added in a 300 ng/ml concentration for JIMT-1 and MDA-MB-231 and 100 ng/ml for T-47D for a further 5-day treatment. After the treatment ended (6 days total), the spheroids were transferred to the adherent 96-well plates (TPP Techno Plastic Products GmbH, Klettgau, Germany), and cell migration was measured at 0 h, 48 h, and 72 h. Pictures of spheroids were taken using the light microscope Axio Vert.A1 ZEISS Zen 2.6 software (Carl Zeiss Microscopy GmbH, Jena, Germany). The area of migrated cells was calculated by the ImageJ/Fiji software, and the results are presented as the difference between the spheroid area at time 0 h and 48 h/72 h in pixels² (mean ± SEM).

2.5. Apoptosis assay and confocal microscopy

The effect of combined DAC and DOX treatment on 3D cell cultures was assessed by confocal microscopy of fluorescently stained spheroids exposed to the same drug concentrations as in the migration assay described above. Apoptotic cells were stained with IncuCyte® Caspase-3/7 Green Dye (Essen BioScience, Newark Close, UK) (0.2 µl/200 µl medium) two days after the last treatment dose (day 6 post-seeding). At the end of the treatment (day 9 post-seeding), the cell nuclei were stained by NucBlue® Live ReadyProbes® Reagent (Thermo-Fisher Scientific, Waltham, MA, USA) (2 drops/ml) for 1–3 h at 37 °C in the incubator.

The images were acquired using the confocal microscope Leica TCS

SP8 STED 3x (Leica Microsystems GmbH, Wetzlar, Germany) with 20x HC PL APO CS2 (NA = 0.75) water objective. The confocal system was adjusted with a pinhole with a diameter of 113 μm . The fluorescence of Incucyte® Caspase-3/7 Green dye was registered with excitation/emission spectra set at 537 nm/550–620 nm and NucBlue® Live ReadyProbes® signal at 492 nm/500–527 nm. The xy-images were recorded by bidirectional scanning with frequency 600 Hz to 2048 \times 2048 pixels and 8-bit grayscale images. The z-stacks of spheroids had thickness from 80 μm with a system optimized step size (around 1 μm) calculated by spectral characteristics and used objective. The spheroid images represented the maximal projections of all stack images.

2.6. Genotoxicity testing by the comet assay

DNA strand breaks (SB) were detected by the standard alkaline comet assay, and oxidized base lesions were measured by nucleoids incubation with formamidopyrimidine DNA glycosylase, Fpg (a kind gift from Norgenotech AS, Norway), as previously described [22,23]. Data are reported as cumulative damage, SB + Fpg. At least three independent experiments were performed, with samples run in duplicate. Briefly, exposed cells were embedded in low-melting-point agarose on microscope slides and incubated for 1 h in lysis solution (2.5 M NaCl, 0.1 M EDTA, 10 mM Tris, 10% v/v Triton X-100, pH 10, 4 °C). The samples used for the Fpg modified assay were washed twice in buffer F (40 mM HEPES, 0.1 M KCl, 0.5 mM EDTA, 0.2 mg/ml BSA, pH 8, 4 °C), and incubated with the Fpg in a humid box at 37 °C for 30 min. All slides were incubated for 20 min in the electrophoresis solution (0.3 M NaOH, 1 mM EDTA, pH > 13 4 °C) to unwind the supercoiled DNA, before being subjected to electrophoresis at 4 °C for 20 min (25 V, 1.25 V/cm, Consort EV202). Finally, the slides were washed in PBS and H₂O and left to dry before staining with SYBR gold (Sigma-Aldrich, USA). Scoring of the nuclei was performed blindly on a fluorescence microscope (DMI 6000 B, Leica Microsystems, Germany) equipped with a SYBR photographic filter (Thermo Fischer Scientific, USA) and the Comet Assay IV 4.3.1 software (Perceptive Instruments, UK). Fifty comets were scored per gel and thus, 100 comets were analyzed per treatment group. The median of the percentage of DNA in the tail was taken as a measure of DNA damage. Data are presented as mean \pm SEM. Slides exposed to H₂O₂ (100 μM , Sigma-Aldrich, Germany), and cells exposed to the photosensitizer Ro 19–8022 (2 μM , kindly provided by Hoffmann La Roche) and light irradiated, were used as PCs for the test performance and the Fpg activity, respectively.

2.7. Whole transcriptome and whole-genome methylation screening experiments

For the whole-transcriptome and whole-genome methylation screening experiments, 2D cells were seeded on Petri dishes (60 mm) at a 300×10^3 cells/dish density and treated with DAC (1 μM for JIMT-1 and 4 μM for T-47D) every 24 h in a total of 72 h. Afterward, the cells were pelleted for molecular analyses. The Human Infinium Methylation EPIC Bead Chip array, measuring 850,000 methylation sites, was used according to the manufacturer's instructions to assess differentially methylated regions (DMRs). Individual methylation value (β value) was evaluated for each CpG site, ranking from 0 for unmethylated to 1 for fully methylated CpGs. The only CpGs located within regions up to 2000 bp upstream and 1000 downstream of transcription start site were analyzed. Whole transcriptome expression was monitored using the BGI DNBSeq PE100 RNA-seq platform.

2.7.1. RNA-seq analysis

Further analysis of RNA-seq data was performed through the application of an analytic workflow including STAR [24], HTSeq [25], and DESeq2 [26] algorithms. STAR aligner was used to map the reads to the Hg38 reference genome, while HTSeq-count was used for gene quantification and generating gene expression counts. Differential gene

expression analysis was implemented using DESeq2, with $\text{abs}(\log_2\text{-FoldChange}) = 1.0$ and $\text{FDR} = 0.05$ as cut-off thresholds of statistical significance.

2.7.2. Methylation analysis

Infinium EPIC methylation arrays were processed via a pipeline including the R ChAMP package [27]. Data were normalized through a BMIQ (beta-mixture quantile) procedure and corrected for batch effect through the ComBat algorithm [28]. By applying the Bumphunter algorithm with adjusted p-value = 0.01 as a significance threshold, DMRs between the control and the DAC-treated samples were identified, revealing a quantitative alteration in DNA methylation levels. Next, each DMR was annotated with its distance to the nearest Transcriptional Start Site (TSS) and the corresponding Gene, using the genomation package [29]. DMRs located in gene promoter regions, up to 2 kb upstream and 1 kb downstream of TSS were kept.

2.7.3. Integration of whole-genome methylation and transcriptomic expression data

In order to explore whether hypermethylation of promoter regions is associated with repressed gene expression and vice versa, the above results of RNA-seq and methylation analysis were compared. To assess their correlation, the least-squares linear regression model was fitted to all the genes based on their methylation and expression $\log_2\text{FoldChange}$ values.

2.7.4. Pathway analysis and gene prioritization

Functional analysis and gene prioritization were performed through the BioInfoMiner web platform (<https://bioinforminer.com>) [30,31]. BioInfoMiner implements topological analysis of data-driven, dynamic, semantic networks derived from four biological vocabularies with an ontological, tree structure: Gene Ontology [32], Human Phenotype Ontology [33], and Mammalian Phenotype Ontology [34] and the REACTOME pathway database [35]. Starting from the initial significant gene list, BioInfoMiner delineates the respective ontological graph by applying graph-theoretic correction of the annotation bias, inherently induced in hierarchical term structures. Then, it performs robust enrichment analysis to prioritize statistically impartially meaningful, biological groupings from trivial findings and ranks genes as putative regulators according to their connectivity in the corrected semantic network [31–36]. Systemic processes are defined as clusters of terms that share maximum semantic similarity and gene content among them but minimize similarity among other clusters. As a result, highly ranked genes are associated with many systemic processes, and thus, are considered as putative hubs in the functional network, assuring homeostatic crosstalk among distinct cellular processes.

2.8. In vivo study

1.25×10^6 JIMT-1 cells resuspended in 100 μl of serum-free DMEM were bilaterally and orthotopically injected into the mammary fat pad of six to eight-week-old female SCID beige mice (SCID/bg, Charles River Germany) to develop orthotopic tumor xenografts. The mice were randomly divided into four groups (four mice per group, the pilot experiment) or six groups (six mice per group, main experiment), and the treatment was initiated when tumors were palpable.

The maximal plasma concentration was used as a key pharmacokinetic parameter for selecting clinically relevant concentrations for the in vivo study [37]. In the pilot experiment, a DOX dose 2 mg/kg body weight (bw) (cumulative dose 4 mg/kg) was used, equivalent to patient dose 6.5 mg/m². The dose conversions were based on the FDA recommendations (Guidance for Industry fda.gov) [38]. Due to severe toxicity, DOX single dose was decreased to 1 mg/kg bw (cumulative dose 4 mg/kg) in the main experiment. The same dose was used for CX, a positive control in this experiment. Dose for DAC (0.125 mg/kg of bw, cumulative dose 1.5 mg/kg) was selected based on the available data for

mice and calculated from a low dose used in human hematologic malignancies treatment, i.e., 15 mg/m²/day [39].

All drugs were administered by intraperitoneal injection (i.p.). DAC was injected 2 or 4 consecutive days per week, while DOX and CX were administered once a week for a total of 4 weeks. The vehicle group was administered with a saline solution. Throughout the experiment, tumors were measured by a caliper, and volume was calculated based on the following formula: tumor volume (mm³) = 0.52 × ((width + length)/2)³. Seven days after the last therapeutic dose, the mice were sacrificed. The results were evaluated as the mean of tumor volumes or tumor weights ± SEM.

2.9. Histology and immunohistochemistry

JIMT-1 cells were trypsinized, centrifuged, washed in serum-free DMEM, and centrifuged to form a compact pellet, fixed in formalin. Tumor xenografts from the experimental animals were immediately fixed in 10% neutral buffered formalin (pH 7.4) for 48 h. After fixation, tissue samples were cut into two halves, and together with the cell line preparation, they were routinely processed in paraffin. Then, 4 μm thick sections were stained with hematoxylin and eosin (HE) for basic morphological evaluation. Histological slides of the tumors were digitized using the EOS1000D camera (Nikon) and morphometrically evaluated using the ImageJ ecosystem software (NIH, Bethesda, USA). The area of the tumor section was evaluated in mm². The extent of tumor necrosis was expressed as a percentage of the cross-section area of the evaluated tumor.

For immunohistochemistry, slides with paraffin sections were deparaffinized, rehydrated, and processed for antigen retrieval in PT-Link (DAKO, Glostrup, Denmark) with citrate buffer, pH 5. The slides were stained using the FLEX system with prediluted ready-to-use antibodies against ER, PR, HER2, and Ki-67 (Agilent, Santa Clara, CA, USA) in the Dako Autostainer (DAKO) according to the manufacturer's instructions. Immunoreactivity was detected with the EnVision™ horse-radish peroxidase kit and visualized by 3,3'-diaminobenzidine (Agilent Technologies). Ki-67 was evaluated using the Zeiss AxioVert 200 microscope (Carl Zeiss Microscopy GmbH, Jena, Germany). The percentage of Ki-67 expression in vital cells was calculated in two areas per slide using Zen 2.6 software (Carl Zeiss Microscopy GmbH, Jena, Germany).

2.10. Quantitative real-time PCR

Total RNA was purified from up to 30 mg of tumor tissue using the RNeasy Mini Kit (Qiagen, Santa Clarita, CA, USA). On-column DNase digestion step with the RNase-Free DNase Set (Qiagen, Hilden, Germany) was included following the manufacturer's protocol. The quality and quantity of extracted mRNA were assessed by NanoDrop® ND-1000 spectrophotometer (Thermo Scientific, Wilmington, DE, USA). A total of 2 μg of RNA from each sample was reverse transcribed using a Revert Aid™ H minus first-strand cDNA synthesis kit (Thermo Scientific, UK). For quantitative real-time PCR (qPCR) TaqMan gene expression assays *CDA* (Hs00156401_m1), *TET1* (Hs00286756_m1), *DNMT1* (Hs00945875_m1), *DNMT3A* (Hs01027166_m1), *DNMT3B* (Hs00171876_m1) were employed. *HPRT1* (Hs02800695_m1) or *GAPDH* (Hs99999905_m1) assays were applied for normalization. The 20 μl reaction mixture consisted of 1 × (10 μl) of Taq-Man gene expression master mix (ThermoFisher Scientific, UK), 1 × (1 μl) Taq-Man® Assay, and 50 ng cDNA template and ultrapure DNase/RNase-free water. *DCK* expression was quantified using individually designed primers (0.5 μM), 1 × GoTaq® qPCR Master Mix (Promega, Madison, WI, USA), 50 ng of cDNA, and ultrapure DNase/RNase-free water. *HPRT1* was employed as a reference gene for normalization. Primer sequences were as follows: *DCK* forward 5'-TCTGAGGGACCCGCATCAA-3', *DCK* reverse 5'-TGCACCATCTGGCAACAGTT-3' (product size 133 bp) and *HPRT1* forward 5'-GGACTAATTATGGACAGGACT-3'; *HPRT1* reverse 5'-GCTCTTCAGTCTGATAAAATCTAC-3' (product size

194 bp). All reactions were run in triplicates on a Bio-Rad CFX96 real-time PCR detection system (Bio-Rad, Hercules, CA). The cycling conditions for TaqMan gene expression assays were as follows: hold 50 °C 2 min for UNG incubation, hold 95 °C 10 min for polymerase activation and 40 cycles denaturation at 95 °C for 15 s followed by annealing/extension step 60 °C for 60 s. For amplification of *CDA* and *HPRT1* genes, cycling conditions were as follows: 50 °C for 2 min, 95 °C for 10 min and 40 cycles at 95 °C for 15 s followed by 60 °C for 30 s and 72 °C for 30 s. The Cq values obtained were then used to quantify relative gene expression employing relative expression software tool REST (REST 2009-RG Mode, Qiagen, Hilden, Germany) developed by Pfaffl et al. [40].

2.11. Global DNA methylation analysis

Genomic DNA was extracted from tumor tissues using a NucleoSpin Tissue Mini kit (Macherey-Nagel, Hoerd, France). DNA concentration and purity were measured by NanoDrop® ND-1000. 2 μg of DNA were used for bisulfite modification using EpiTect Bisulfite Kit (Qiagen, Hilden, Germany). Global DNA methylation was assessed by quantifying the long interspersed nucleotide element 1 (LINE-1) methylation level. Analysis of LINE-1 methylation level was performed by pyrosequencing, a gold standard method for quantitative detection of DNA methylation. PyroMark Q24 CpG LINE-1 kit (Qiagen, Hilden, Germany) was used for PCR amplification of 146 bp PCR product, allowing for analysis of three CpG sites in positions 331–318 of the LINE-1 sequence (GenBank accession no. X58075). Pyrosequencing runs were carried out using a PyroMark Q24 system and the PyroMark Gold Q24 Reagents (Qiagen, Hilden, Germany) following the manufacturer's protocol. Data analysis was performed by PyroMark Q24 2.0.6. software (Qiagen, Hilden, Germany). The results are presented as the average methylation percentage in three CpG sites.

2.12. Western blot

Proteins were isolated from tumor tissues using RIPA lysis buffer (Cell Signaling Technology) supplemented with Complete™ Protease Inhibitor Cocktail (Roche) and PhosSTOP™ (Roche) phosphatase inhibitor. Total protein concentration was quantified by Pierce™ BCA Protein Assay Kit (Thermo Scientific). Protein samples were diluted in 4 × Laemmli Sample Buffer (Biorad) and heated for 10 min at 90 °C before use. Equal amounts of proteins were separated by 7.5–10% SDS-PAGE and transferred by wet blotting to nitrocellulose membrane (Thermo Scientific, Germany). Membranes were blocked in 5% w/v non-fat dry milk (Artifex Instant s.r.o. Czech Republic) in TBS (20 mM Tris, 150 mM NaCl) and incubated with DNMT1 (D63A6) XP® Rabbit mAb (1:1000) (Cell Signaling Technology, cat.no. 5032) or anti-β-actin mouse monoclonal (1:4000) primary antibody (Sigma Aldrich, cat.no. A1978). Membranes were washed in TBS-T (20 mM Tris, 150 mM NaCl, 0.1% Tween 20) and incubated in corresponding secondary antibodies Goat anti-Rabbit IgG (H + L) Highly Cross-Adsorbed Secondary Antibody, Alexa Fluor 680 (1:10 000) or Goat anti-Mouse IgG (H + L) Highly Cross-Adsorbed Secondary Antibody, Alexa Fluor 680 (1:10 000) (Thermo Scientific). Visualization was performed using Odyssey® Fc (LI-COR) imaging system. Levels of detected proteins were quantified by densitometry using ImageJ/Fiji software and expressed as protein/loading control ratio relative to vehicle control.

2.13. Statistical analysis

Normality of distribution was tested using Shapiro–Wilk test. Significant differences between normally distributed data were assessed by Student t-test or one-way analysis of variance (ANOVA) and appropriate post hoc tests depending on assumed variances. Non-normally distributed data were evaluated using Mann-Whitney U-test or Kruskal–Wallis test followed by Dunn or Dunn–Bonferroni post hoc methods. A general

linear model for repeated measures with Greenhouse-Geisser correction, if a violation of sphericity was assumed, was used to evaluate the effects of particular treatment types over individual time points. The analysis of covariance was used to examine the association between the treatment and tumor necrosis, with tumor size as a covariate. Data were analyzed

using the SPSS software package version 23 (IBM SPSS, Inc., Chicago, IL, US) and GraphPad Prism 8.0.1 for Windows (GraphPad Software, San Diego, CA, USA). CalcuSyn Software (Biosoft, Cambridge, UK) was applied to calculate CI and IC₅₀ values. Differences with $p < 0.05$ were considered to be statistically significant.

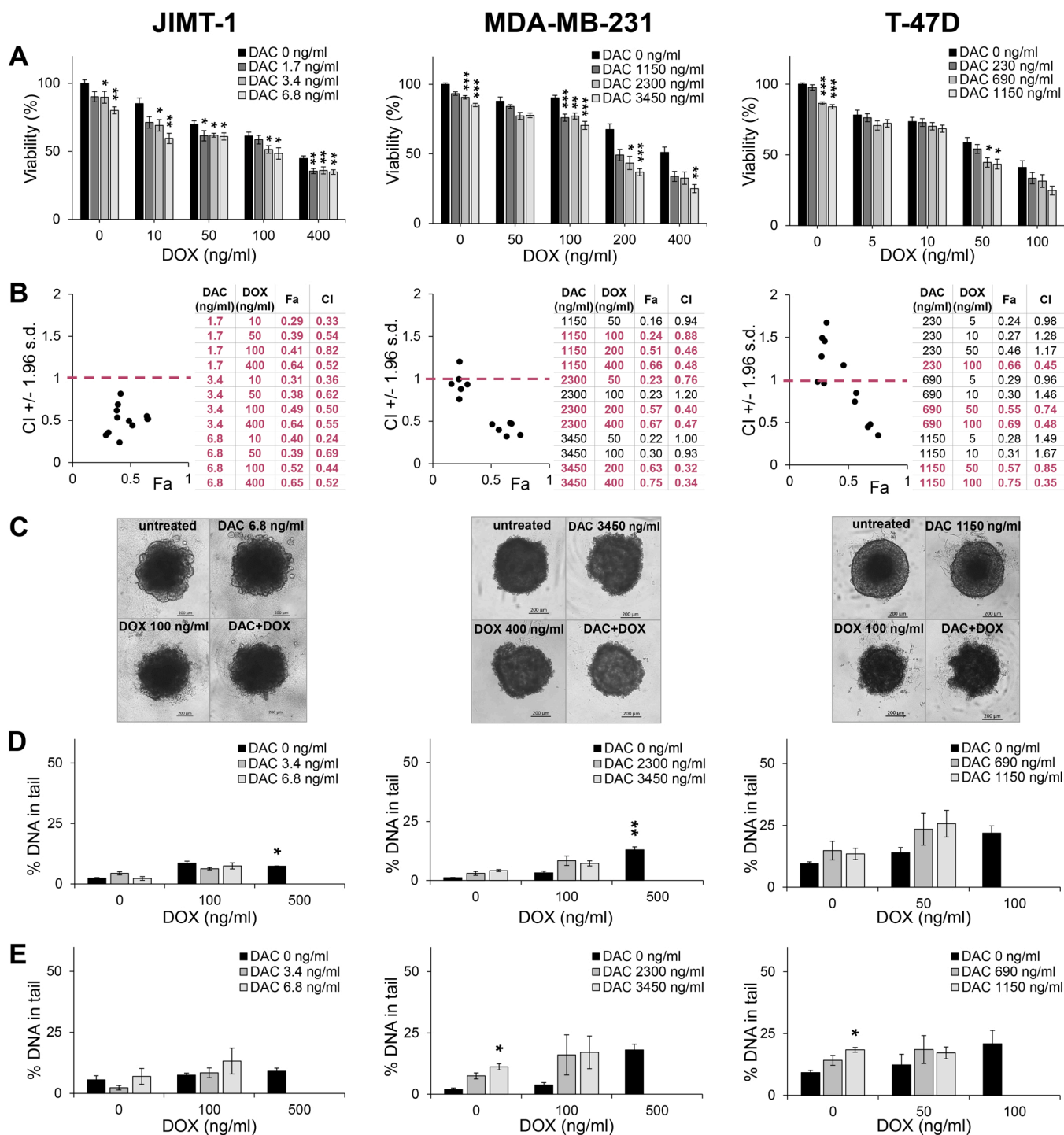


Fig. 1. The effect of combined sequential treatment with decitabine (DAC) and doxorubicin (DOX) on BC cells cultivated as 3D spheroids. (A) Relative cell viability values are expressed as means \pm SEM from three independent experiments calculated relative to the negative control (set to 100%). Difference to DOX single treatment; * $p < 0.05$, ** $p < 0.01$, *** $p < 0.001$; (B) Interactions between DAC and DOX calculated by CalcuSyn software and expressed as combination index (CI). CI on the y-axis is a function of fraction affected (Fa) on the x-axis (Fa = 1 - % of viable cells/100). Synergism (CI < 1), additivity (CI = 1), or antagonism (CI > 1) are expressed in Fa-CI plots for the entire spectrum of drug combinations; (C) Representative images of control spheroids and those treated with DAC, DOX, and DAC + DOX; Magnification 5 \times ; (D) The level of strand breaks (SB) and (E) oxidized base lesions (data reported as cumulative damage, SB + Fpg) after DAC, DOX and DAC + DOX treatment assessed by comet assay. Data are presented as mean values from 3 independent experiments \pm SEM; * $p < 0.05$, ** $p < 0.01$. SB + Fpg were significantly different from SB only in MDA-MB-231 cells at the highest concentration of DAC ($p = 0.008$).

3. Results

3.1. DAC pre-treatment potentiated the toxic effect of DOX in vitro

To comprehensively evaluate the potential benefit of combined DAC + DOX exposure, we performed a set of in vitro experiments. The efficacy of the sequential combined treatment was compared with the effects of DAC or DOX alone in JIMT-1, MDA-MB-231, and T-47D BC cell lines, cultivated in 2D conditions and as 3D multicellular spheroids. Substantial differences in sensitivity to DAC and DOX were identified among BC cell lines growing as adherent cell cultures (Table S1). The most sensitive to DAC treatment were JIMT-1 cells ($IC_{50} = 0.03 \mu\text{g/ml}$), followed by MDA-MB-231 ($IC_{50} = 0.09 \mu\text{g/ml}$) and T-47D ($IC_{50} = 1.24 \mu\text{g/ml}$). While JIMT-1 cell line was the most resistant to DOX ($IC_{50} = 0.05 \mu\text{g/ml}$), the sensitivity of MDA-MB-231 and T-47D cells was identical ($IC_{50} = 0.02 \mu\text{g/ml}$). At selected sub-cytotoxic concentrations (Fig. S1A, Table S2), DAC did not significantly increase the SB levels after 24 h treatment (Fig. S1B). However, in JIMT-1 cells, a significant and dose-dependent elevation of oxidized DNA lesions was found. Results for SCs and PCs are reported in Table S3. On the other hand, the chronic exposure to DAC induced a concentration-dependent reduction of viability in all BC cell lines (Fig. S1C).

Remarkably, spheroids mimicking more closely the complex micro-environment in vivo were more resistant to DAC and DOX exposure. In agreement with the 2D results, the most sensitive to DAC were JIMT-1 spheroids ($IC_{50} = 0.49 \mu\text{g/ml}$), followed by T-47D ($IC_{50} = 2.73 \mu\text{g/ml}$) and MDA-MB-231 ($IC_{50} = 3.55 \mu\text{g/ml}$). Nearly one order of magnitude higher concentrations of DOX had to be used to reach comparable cell survival as in 2D cell cultures for JIMT-1 and MDA-MB-231 cells ($IC_{50} = 0.23 \mu\text{g/ml}$, and $0.27 \mu\text{g/ml}$, respectively), while IC_{50} value for T-47D cells was $0.09 \mu\text{g/ml}$ (Table S1).

Three sub-cytotoxic DAC concentrations (around IC_{20}) were selected and combined with five DOX concentrations ranging from non-cytotoxic to toxic (viability from 100% to 20%) to evaluate the ability of DAC to sensitize BC cells towards DOX. The effect of combined exposure resulted in a dose-dependent inhibition of cell viability under both 2D and 3D conditions (Figs. S2A, 1A). A synergistic effect ($CI < 1$) was identified at several DAC + DOX concentrations in all cell lines (Figs. S2B, 1B). Cell pre-treatment with low DAC (IC_{20}) concentrations followed by exposure to DOX (IC_{50}) inhibited the cell proliferation more efficiently than DOX alone (Fig. S2C). In line with these results, a significant reduction of cell survival after DAC + DOX treatment was confirmed by CFE assay (Fig. S2D). Combined treatment at selected concentrations did not significantly increase DNA damage measured as SB (Fig. S2E) or SB+Fpg (Fig. S2F) in the 2D cultures. Results for SCs and PCs are reported in Tables S2–S4.

Interestingly, CX was less cytotoxic at equivalent concentrations than DOX in all BC cell lines (Fig. S3). However, JIMT-1 cells, the most resistant to DOX, were also the most resistant to CX ($IC_{50} = 0.77 \mu\text{g/ml}$), followed by MDA-MB-231 and T-47D ($IC_{50} = 0.15 \mu\text{g/ml}$, and $IC_{50} = 0.29 \mu\text{g/ml}$, respectively) (Table S1). Most DAC + CX combinations also showed synergistic effects.

In the model of 3D spheroids, the benefit of sequential combined treatment was most pronounced in JIMT-1 cells, where all tested combinations showed synergy, followed by MDA-MB-231 (Fig. 1B). However, relatively high concentrations were used due to the low sensitivity of MDA-MB-231 and T-47D cells to DAC. Only a few DAC + DOX combinations were found synergistic in the T-47D spheroids. Representative images of the spheroids treated by the synergistic drug combination are shown in Fig. 1C. Single DOX treatment revealed a significant increase in SB only at a cytotoxic concentration of 500 ng/ml in JIMT-1 and MDA-MB-231 spheroids (Fig. 1D). Significant induction of oxidized base lesions was observed at the highest concentration of DAC single treatment in MDA-MB-231 and T-47D spheroids. However, no significant induction of SB or oxidized base lesions was detected after combined treatment (Fig. 1E). Results for SCs and PCs are reported in

Tables S2 and S3.

Furthermore, cell apoptosis and migration ability were evaluated to follow the cellular processes underlying the synergism between DAC and DOX. Immunofluorescent staining revealed a rise in the number of apoptotic cells only in T-47D spheroids after combined DAC + DOX treatment (Fig. 2). In contrast, apoptotic cells were abundant in JIMT-1 spheroids, with the most intensive apoptotic signal in the central part, even in untreated controls. Therefore, the contribution of single or combined treatment to increased apoptosis was hard to elucidate in this cell line. On the other hand, the MDA-MB-231 cells remained relatively resistant to all treatment types.

The anti-migratory effect of DAC + DOX exposure was also assessed on the spheroid models, more closely reflecting the solid tumor micro-environment. The spheroids were treated with the same concentrations of DAC, DOX, and DAC + DOX as for the apoptosis assay. Images were taken 72 h (JIMT-1 and T-47D cells) and 48 h (MDA-MB-231 cells) post-transfer from non-adherent to adherent conditions to facilitate the migration of cells shedding from the spheroids. We identified high migratory capacity in untreated JIMT-1 and MDA-MB-231 cells significantly lowered after DOX single- and combined treatment (Fig. 3), while it was relatively low in T-47D cells.

3.2. Sensitive and resistant cells differ in their transcriptome and methylome signatures and response to DAC treatment

To better understand the increased sensitivity of JIMT-1 cells to DAC exposure, an integrative approach with genome-wide DNA methylation (Infinium Methylation EPIC array) and a transcriptomic analysis (RNA-Seq) was applied (Fig. 4). Two pyrimidine metabolism enzymes, deoxycytidine kinase (DCK) and cytidine deaminase (CDA), are critical in DAC metabolism (Fig. 4A). Therefore, we assume that their interplay with DNA methylation machinery (DNMT enzymes and TET family of dioxygenases) and molecular differences between cell lines can significantly influence response to DAC. The transcriptomic and methylomic signatures of both untreated (Fig. 4B–D) and DAC-exposed (Fig. 4E, F) T-47D and JIMT-1 cells were compared. An extensive number of differentially expressed genes (DEGs) were identified between untreated cells, in total over 6000 transcripts, 3217 in T-47D and 3150 in JIMT-1 cells when 2-fold difference and p-value less than 0.05 were set as a cut-off (Fig. 4B; Table S5). The top DEGs were *PARVA*, *AXL*, *FAM83A*, *TPM4*, *COL6A1*, *ZFP36L2*, *ADAM19*, *ANKRD13A*, *ADAMTSL4*, *ETV4*, *ETS2*, *LAMC2*, *MUC1*, *FOXA1* (the complete list of upregulated and down-regulated genes in JIMT-1 vs. T-47D cells, including adjusted p-values and $\log_2\text{FoldChange}$ is provided in Table S5). By implementing a robust integrative bioinformatic analysis of transcriptomic data using Bio-InfoMiner platform, from 256 prioritized DEGs (Fig. 4C), consensus signatures of 184 linker genes were identified. Out of these, 56 were upregulated in a T-47D cell line with the top candidates *ESR*, *AR*, *IRS1*, *RARA*, *AKT1*, and *FGFR2* involved in several cancer pathways, including insulin receptor, IL-2 and IL-4, and FGF signaling. The remaining 128 genes were upregulated in JIMT-1 cells with highly ranked *EGFR*, *CAV1*, *TGFBR2*, *CD44*, *PPARG*, *JUN*, *FYN*, or *LYN* genes enriched in EGFR1, axon guidance, focal adhesion, extracellular matrix organization, receptor interaction, or signal transduction pathways. Moreover, significant differences between cell lines were found in the expression of genes encoding enzymes and epigenetic regulators crucially involved in DAC metabolism and DNA methylation, namely *CDA*, *DNMT3B*, *TET1*, and *TET3* ($p = 1.0 \times 10^{-22}$, $p = 3.8 \times 10^{-17}$, $p = 5.9 \times 10^{-6}$ and $p = 7.4 \times 10^{-1}$, respectively). While nearly 3000-folds upregulated expression of CDA was detected in the JIMT-1 cell line, *DNMT3B* and *TET1* were downregulated, as confirmed by qPCR validation (Fig. 4D). The expression of *DCK*, *DNMT1*, and *DNMT3A* did not differ significantly.

Interestingly, after 72 h exposure to DAC (approx. IC_{20} , added every 24 h due to its low stability), we found a 60-fold increase of CDA expression in T-47D cells, while no treatment effect was found in JIMT-1

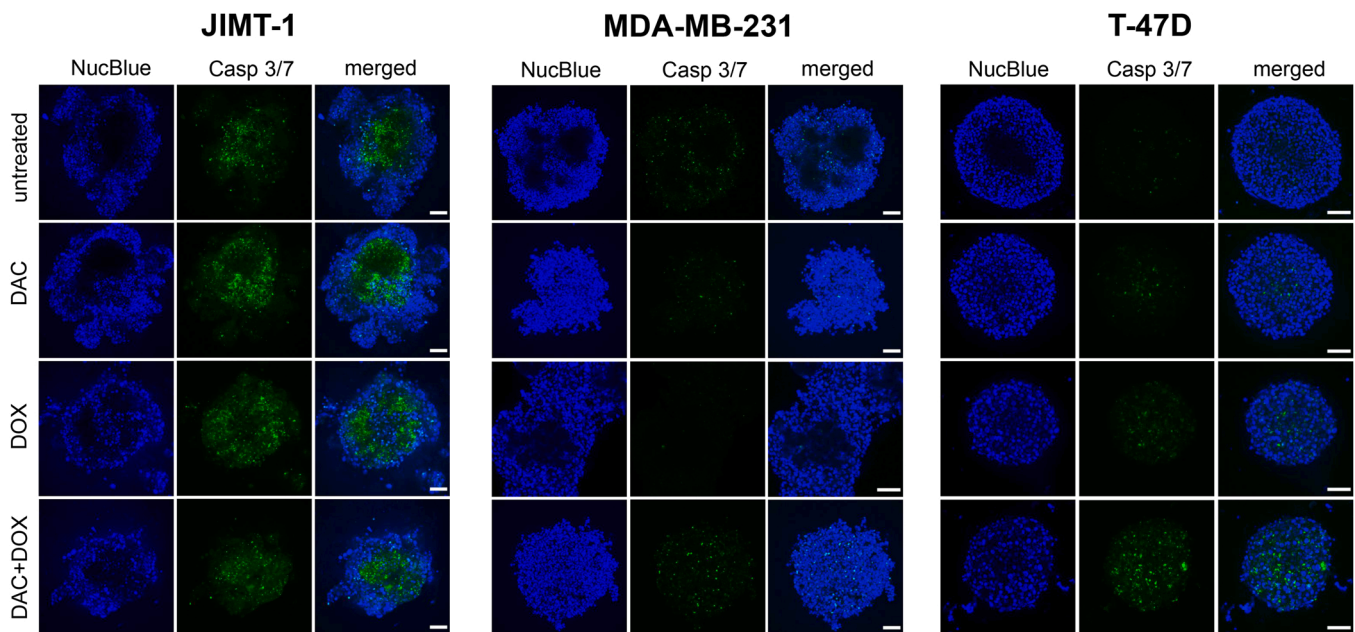


Fig. 2. Treatment-induced apoptosis in BC spheroid models visualized by confocal microscopy. JIMT-1, MDA-MB-231, and T-47D spheroids were sensitized for 24 h with 3.4 ng/ml, 2300 ng/ml, and 690 ng/ml DAC, respectively, followed by 5-day treatment with 300 ng/ml DOX for JIMT-1 and MDA-MB-231, and 100 ng/ml for T-47D. Representative images were taken 9 days post-seeding and presented as the maximal projection of all xy-images gained in volume with a thickness of more than 80 μ m. Spheroids were labeled with NucBlue (blue) to show cell nuclei and Caspase-3/7 (green) as a late apoptosis marker. All scale bars are 100 μ m; Magnification 20 \times .

cells. The change of *DCK* expression was below 2-fold cut-off, similar in both cell lines (Fig. S4). DAC-induced decrease of DNA methylation was accompanied by upregulation of gene expression in the set of significantly differentiated genes (197 in T-47D cells and 168 in JIMT-1 cells), with 66 common genes for both cell lines (Fig. 4E). Gene prioritization analysis revealed cell-line specific signatures, involved in distinct pathways. The most significant changes in T-47D cells were found for genes involved in the cell differentiation, cell fate commitment, actin filament organization, extracellular structure, or cell-substrate adhesion pathways, including *BCL2*, *CAV1*, *THY1*, *NRXN1*, *LOX*, *LOXL2*, *FGF2*, *ACTIN1*, *DKK1* or *ITGA4* genes (Fig. 4F, Fig. S5). In JIMT-1 cells, the top prioritized linker genes were *TNF*, *CACNA1A*, *DLL1*, *WNT1*, *SMPD3*, *DKK1*, *ABCG1*, *TNFRS18*, *CDH13*, and *GHR* (Fig. 4F, Fig. S6), with the top enriched developmental pathways.

Furthermore, DAC-induced expression changes of HER2 and selected genes involved in trastuzumab resistance, namely *MUC1*, *EGFR*, and *CD44*, were extracted from the transcriptomic data (Table S6). DAC exposure induced a 2.3-fold upregulation of *MUC1* in JIMT-1 cells, almost halving *EGFR* mRNA expression, while *ERBB2* and *CD44* changes remained below cut-off values in both cell lines.

3.3. Combination therapy reduced the tumor growth, decreased DNA methyltransferases gene expression and global DNA methylation in orthotopic xenografts

Based on the in vitro results, the trastuzumab-resistant JIMT-1 cell line was used to induce orthotopic BC xenografts in immunodeficient mice. Female SCID beige mice were injected bilaterally and orthotopically into the mammary fat pad with JIMT-1 cells. The status of ER-, PR-, HER2+ expression was verified both in JIMT-1 cells and in xenografts (Fig. S7A, B). The JIMT-1 cell culture pellet was composed of rounded cells showing pleomorphism, atypia, and high mitotic rate. The immunocytochemical profile showed ER-, PR-, HER2 2+ (20% cells with weak complete membrane positivity). The tumor xenografts' histomorphology corresponded to invasive breast adenocarcinoma, no special type (NST), Grade 2 (WHO 2018), prevalently with solid growth pattern

(Fig. S7B). Structures of the original mammary gland were not observed. The tumors' immunohistochemical profile (ER, PR, and HER2 expression) was identical to that of the cell line and did not show changes related to different therapeutic schemes. The pilot experiment was performed with four mice per group to optimize the dose and the administration schedule. DAC (0.125 mg/kg i.p.) and DOX (2 mg/kg i.p.) were administered repeatedly as monotherapy or in combination following the schemes depicted in Fig. S8A, B. As DOX in this concentration caused severe toxicity, the experiment had to be prematurely terminated on day 31 (day 16 of the treatment). Combination therapy in the pilot experiment induced a significant decrease in tumor weight ($p = 0.001$) compared to the vehicle group (Fig. S8C). DOX treatment increased tumor necrosis extent when adjusted for tumor size ($p = 0.036$ vs. vehicle group) (Fig. S8D).

In the main experiment, DOX concentration was decreased to the dose of 1 mg/kg bw, while the DAC concentration remained the same (Fig. 5). Moreover, mice exposed to an equivalent concentration of CX and DAC + CX were included as positive controls. The treatment started on day 8 (Fig. 5A, B). The cumulative DOX and CX dose of 4 mg/kg bw was achieved in four consecutive administrations on day 31 (day 23 of the treatment).

Significant reduction in tumor volume was achieved by DAC + DOX combination therapy compared to vehicle ($p = 0.002$) and DOX alone ($p = 0.008$) (Fig. 5B). The weight of DAC + DOX, CX, and DAC + CX treated tumors was significantly lower than those of controls ($p = 0.011$; $p = 0.003$ and $p = 0.010$; respectively) and DAC monotherapy ($p = 0.027$; $p = 0.008$ and $p = 0.027$; respectively) (Fig. 5C). Representative images of the tumor xenografts are shown in Fig. 5D. The histomorphological appearance with the extensive areas of central necrosis did not differ significantly between treatment groups (Fig. 5E). Changes in Ki-67 proliferation were evaluated in tumor xenografts (Fig. 5F, G). In contrast to free DOX, CX ($p = 0.006$ vs. DAC and $p = 0.031$ vs. DAC + DOX), especially in combination with DAC ($p = 0.004$ vs. vehicle, $p < 0.001$ vs. DAC, $p = 0.016$ vs. DOX and $p = 0.001$ vs. DAC + DOX), induced a significant decrease of Ki-67 expression in viable tumor cells.

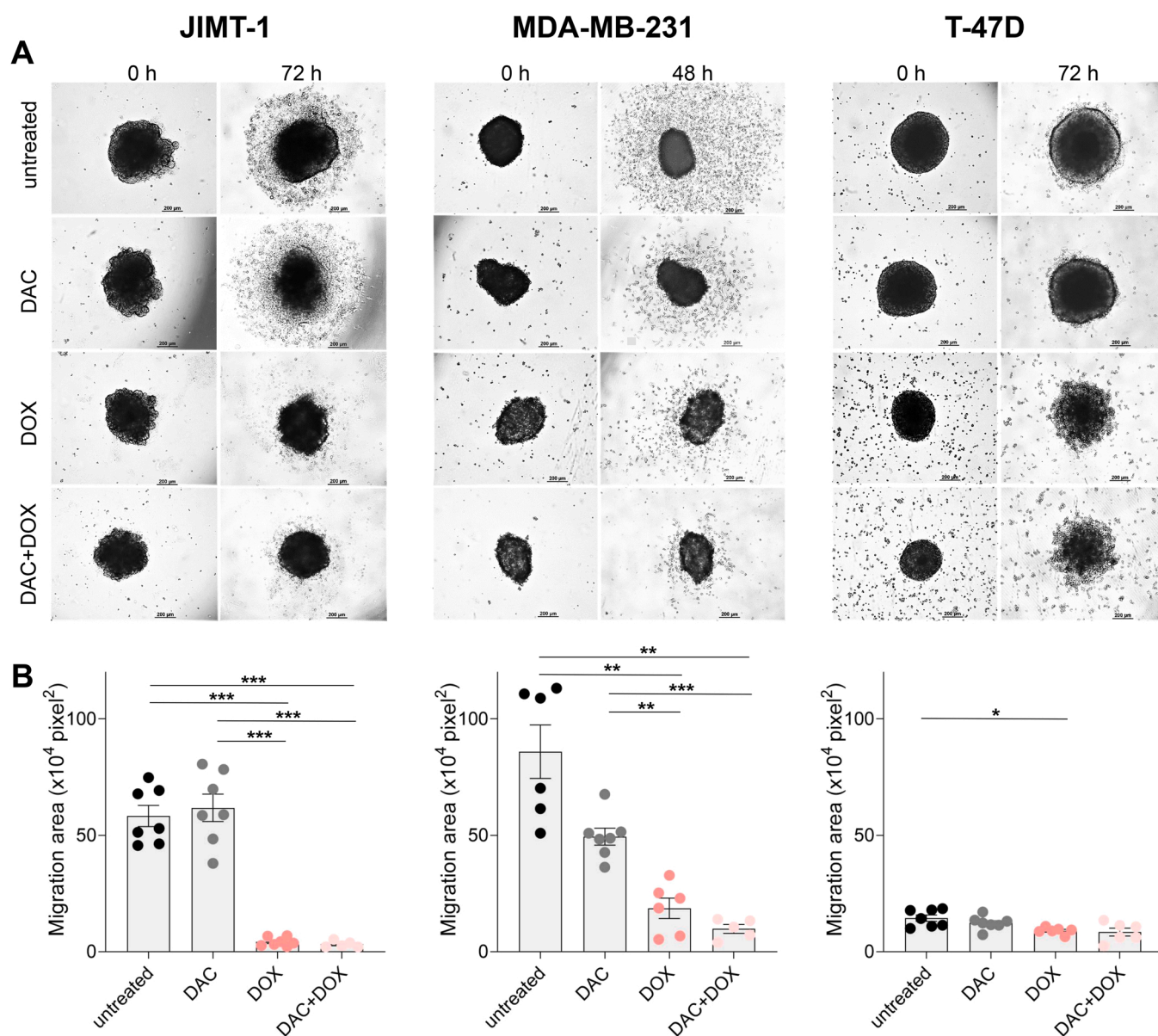


Fig. 3. The cell migration ability of untreated 3D spheroids and after treatment with decitabine (DAC), doxorubicin (DOX), and their combination (DAC + DOX). JIMT-1, MDA-MB-231, and T-47D spheroids were pre-treated for 24 h with 3.4 ng/ml, 2300 ng/ml, and 690 ng/ml DAC, respectively. Subsequently, DOX was added in a 300 ng/ml concentration for JIMT-1 and MDA-MB-231, and 100 ng/ml for T-47D for the following 5-day treatment. (A) Images of spheroids taken by a light microscope at 0 h and 48/72 h after their transfer to adherent plates; Magnification 5 ×; (B) Migration area was calculated using ImageJ/Fiji software as a difference between the area of spheroids at 0 h and spheroids with shed cells at 48/72 h. Values are expressed as means of area differences ± SEM in pixel²; * p < 0.05, ** p < 0.01, *** p < 0.001.

The expression of three DNMTs at mRNA and protein levels, along with global DNA methylation changes, were examined in the tumors of treated animals to assess if the therapeutic effect was mediated by epigenetic regulation. To better illustrate obtained results, fold changes (FCs) instead of log2FoldChanges are described. A significant downregulation of *DNMT1* and *DNMT3B* genes was induced by DAC + DOX (FC = 0.5, p = 0.006; FC = 0.7, p = 0.010, respectively) (Fig. 5H). Low levels of DNMT1 protein detected by Western blot in DAC + DOX treated xenografts (Fig. 5I) confirmed the downregulation of *DNMT1* mRNA estimated by qPCR. On the other hand, DAC treatment caused upregulation of *DNMT3A* (FC = 1.6, p = 0.004). However, the expression of DNMT3A and DNMT3B proteins was low in JIMT-1 cells (data not shown). Accordingly, a significant decrease of LINE-1 methylation was found in tumors of DAC and DAC + DOX treated mice when compared to the vehicle (p = 0.043 and p = 0.003, respectively) and CX

(p = 0.032 and p = 0.002, respectively) groups (Fig. 5J).

In the pilot experiment (Fig. S8), DOX treatment induced a significant downregulation of *DNMT1* gene (FC = 0.5, p = 0.026), while *DNMT3A* and *DNMT3B* gene expression remained unchanged (Fig. S8E). LINE-1 methylation decreased after DAC (p = 0.030) and DAC + DOX (p = 0.009) treatment compared to the vehicle group. A lower level of global DNA methylation against the DOX was also identified in the tumors of DAC (p = 0.044), and DAC + DOX (p = 0.014) treated animals (Fig. S8F).

4. Discussion

New treatment modalities and drug combinations are needed for more aggressive cancer subtypes, such as HER2-positive BC, often resistant to established therapeutic approaches. Trastuzumab is an FDA-

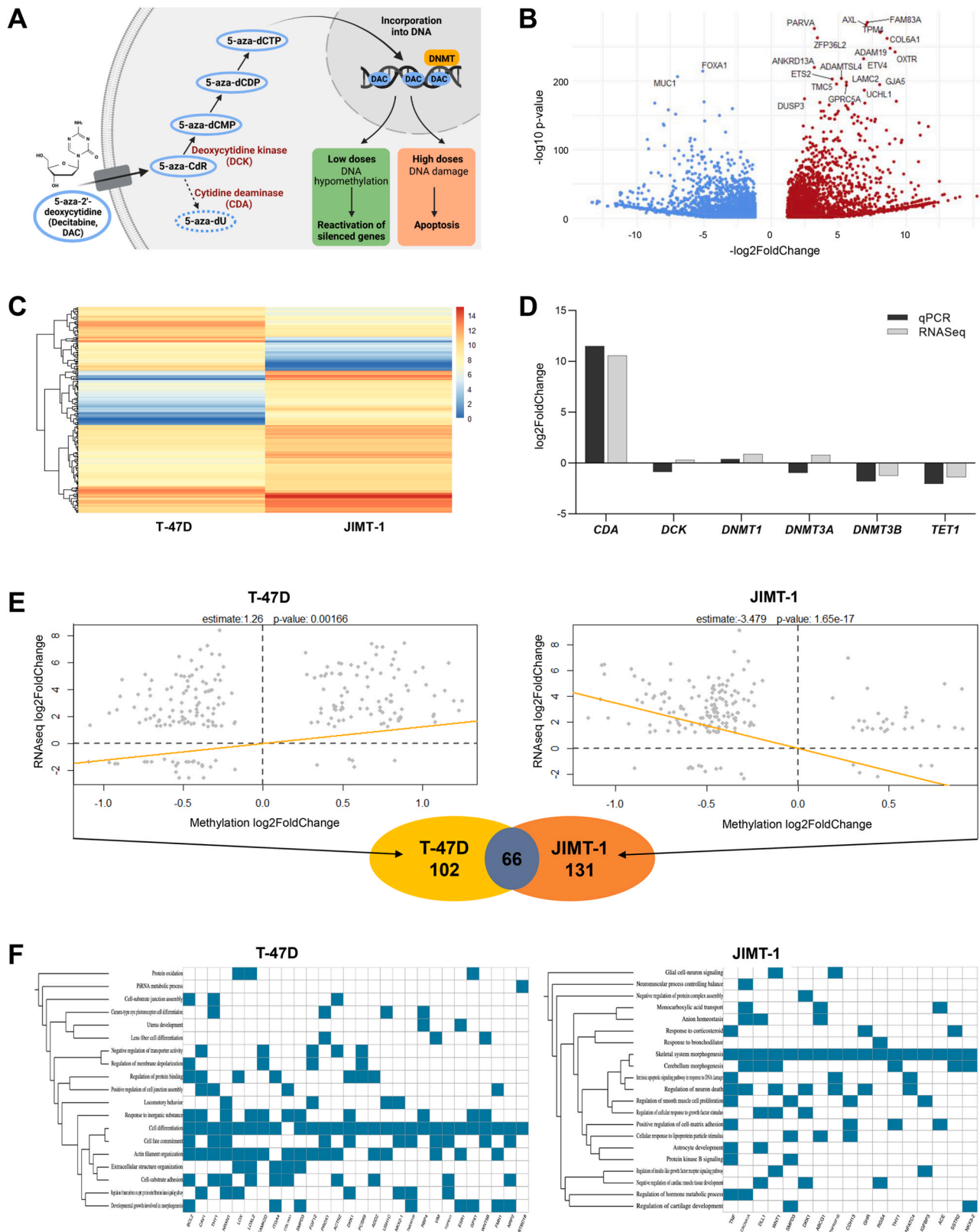


Fig. 4. Genome-wide transcriptomic and methylation analysis for untreated and decitabine (DAC) -exposed T-47D and JIMT-1 cells. (A) Enzymes involved in DAC metabolisms; (B) Volcano plot illustrating differentially expressed genes in trastuzumab-resistant JIMT-1 cell line compared to T-47D cells, blue dots represent downregulated, red dots upregulated genes; (C) Heatmap of 256 prioritized differentially expressed genes (log2 of normalized counts, mean of 3 replicates); (D) Validation of RNASeq data by qPCR for crucial genes involved in DAC metabolism and DNA methylation regulation in JIMT-1 vs. T-47D cells; (E) Correlation plots of differentially methylated and expressed genes in T-47D and JIMT-1 cells exposed to DAC. The Venn diagram shows a number of genes in which expression and methylation levels of the subgroups is anti-correlated (decreased DNA methylation accompanied by upregulated gene expression); (F) Heatmaps for T-47D and JIMT-1 cells exposed to DAC visualizing the mapping of prioritized genes (x-axis) to systemic processes (y-axis).

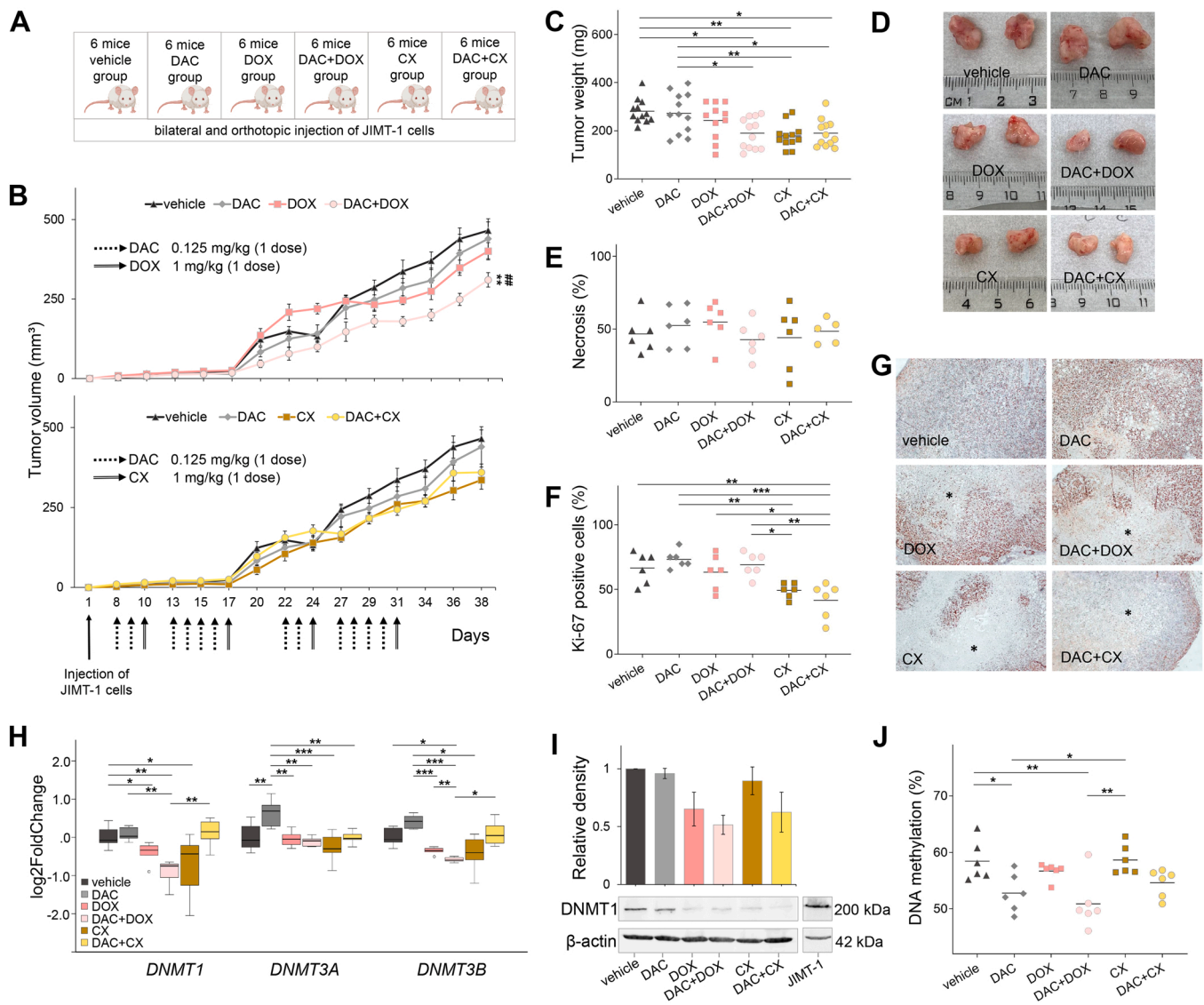


Fig. 5. The therapeutic effect of decitabine (DAC), doxorubicin (DOX), Caelyx® (CX), and their combination (DAC + DOX; DAC + CX) in vivo. (A) Design of the experiment; (B) Treatment schedule and tumor growth; * difference to vehicle group, # difference to DOX group, **, ## $p < 0.01$; (C) Tumor weight at day 38 when mice were sacrificed; (D) Representative images of tumors from each treatment group; (E) Necrosis extent quantitatively evaluated in tumor xenografts; (F) Quantitative evaluation of Ki-67 expression; (G) Immunohistochemical staining of Ki-67 expression in xenografts, including large areas of necrosis (*); (H) Relative gene expression of DNA methyltransferases (*DNMT1*, *DNMT3A* and *DNMT3B*) presented as log₂FoldChange; (I) Representative results of Western blot analysis for DNMT1 expression after individual treatments and quantification by densitometry from 3 experiments; (J) Global DNA methylation level changes in mice tumors after treatment; * $p < 0.05$; ** $p < 0.01$; *** $p < 0.001$.

approved agent used with remarkable results when combined with neoadjuvant chemotherapy against early and locally advanced HER2-positive BC subtype. Unfortunately, about one-third of these patients fail to achieve pathological complete remission, leaving them with few remaining treatment options. Attractive experimental alternatives to sensitize resistant cancer cells to standard therapy include reversing aberrant DNA hypermethylation and associated gene silencing by epigenetic drugs. By testing this approach in vitro, we found synergism between DAC and DOX in all tested BC cell lines cultivated as 2D and 3D spheroids. Surprisingly, the JIMT-1 cells, representing a model of trastuzumab resistance, were the most sensitive to DAC. In contrast to previously published data [41], sensitivity to DAC differed depending on BC subtype. The DAC concentrations selected for combined treatment did not increase the basal level of SBs in any BC cell line, supporting the assumption that the therapeutic effect of low concentration DAC was mediated primarily via DNA methylation changes. However, a significant DNA oxidation rise was found in JIMT-1 cells. The ability of DAC to

induce oxidative stress has already been reported by several authors [42–44]. The observation that no significant genotoxicity was found under combined treatment suggests that the DNA damage might be either repaired or removed via apoptosis.

As determined by the whole-genome approach, the aggressive behavior of JIMT-1 cells, including their high migration potential or tumorigenicity compared to T-47D luminal A cells, can be attributed to the upregulation of genes involved in diverse cellular processes, such as cell adhesion, migration, proliferation, cell-matrix interactions, angiogenesis, epithelial-to-mesenchymal transition (EMT), ubiquitination, invasiveness, stemness, and immune modulation. Our results are consistent with previous findings showing an association between trastuzumab resistance and migratory potential of the cells, specifically in the context of EMT [45,46]. Notably, upregulation of AXL tyrosine kinase, involved in regulating tumor cell plasticity, has been shown a key driver of acquired drug resistance to several anticancer therapies, including trastuzumab [47]. Variations in DAC response between

studied cell lines could also be explained by differences in mRNA expression of *CDA* and DNA methylation enzymes, namely *DNMT3B*, *TET1*, and *TET3*. Pyrimidine metabolism enzymes, including *CDA* and *DKK*, play a crucial role in DAC sensitivity [48,49]. *CDA* has been shown to contribute to DAC resistance in vitro, as it rapidly catabolizes DAC into uridine counterparts that do not deplete DNMT1. Surprisingly, this enzyme was highly expressed in DAC-sensitive JIMT-1 cells, while DAC exposure only augmented its expression in T-47D cells. We can speculate that DAC-inducible upregulation of *CDA* might contribute to higher DAC resistance in T-47D cells. Consistently with our findings, it was demonstrated that DAC substantially increased *CDA* mRNA levels in the 7 *CDA*-deficient cancer cell lines. At the same time, it had little or no effect on *CDA* transcript levels in cell lines, which have constitutively high expression of *CDA* [50].

Distinct pathways were enriched in studied cell lines after DAC treatment. The *TNF* and *CACNA1A* were the highest-rated genes regarding their regulatory capacity and the intensity of their differential expression found in JIMT-1 cells. Recently, a novel apoptosis-inducing mechanism of DAC, mediated by upregulation of TNF- α has been revealed in melanoma cells [51]. Unfortunately, an abundant number of apoptotic cells present in unexposed JIMT-1 spheroids hindered an objective assessment of DAC contribution to the induction of programmed cell death in this cell line. Thus, this mechanism warrants further investigation in HER2-positive cells. *CACNA1A*, a novel promising target for cancer therapy, belongs to voltage-gated calcium channels (VGCCs). Low expression of *CACNA1A* compared with normal tissue is associated with various cancers, including BC [52]. On the contrary, its high expression significantly reduced the cell proliferation capability [53]. Based on these findings, we assume that upregulation of this gene in JIMT-1 cells might contribute to their increased sensitivity. However, we also identified several proto-oncogenes (*WNT1*, *MYC*) and multidrug resistance-related ABC transporter *ABCG1* among the top prioritized genes. These data, including the upregulation of *MUC1* in JIMT-1 cells, indicate that the use of epigenetic regulators for treating solid tumors should be considered cautiously. Targeted delivery over systemic application might be a more efficient therapeutic mode to avoid possible off-target DAC effects [3].

In line with in vitro results, DAC + DOX combination therapy inhibited the growth of trastuzumab-resistant orthotopic BC xenografts. A significant decrease in global DNA methylation confirmed the effect of combination therapy on tumor cell methylome. Reduced tumor growth was accompanied by decreased DNMT1 expression at mRNA and protein levels. DNMT1 is a crucial drug target in triple-negative BC [54]. The expression of this enzyme has been associated with poor BC survival and correlates positively with DAC sensitivity. The oncogenic role of *DNMT1* includes promotion of EMT and metastasis, induction of cellular autophagy, and growth of cancer stem cells. Besides DAC, the intercalation of DOX into DNA can also contribute to DNMT1 inhibition by affecting its catalytic activity, leading to the apoptosis of cancer cells [55]. Traditionally, DNMT1 is considered a maintenance DNMT, while DNMT3A and DNMT3B are accounted *de novo* DNMTs, involved mainly in early development. However, there is increasing evidence supporting the hypothesis of crosstalk between *de novo* and maintenance DNA methylation machinery in several cellular contexts [56]. Yu et al. demonstrated degradation of all DNMTs following low-concentration and long-term DAC treatment in vitro and in vivo, using patient-derived xenograft organoids established from chemotherapy-sensitive and resistant triple-negative BC [57]. Interestingly, DAC monotherapy also caused a slight upregulation of *DNMT3A* and *DNMT3B* genes. Overexpression of *DNMT3B* was associated with increased resistance to the growth-inhibitory effect of DNMTi in pancreatic cancers [58].

Although the combination DAC + DOX therapy did not reach the synergy in vivo, it has shown similar efficacy as CX, considered a safer alternative to DOX [59]. This pegylated liposomal DOX formulation is used, mainly due to its high cost, exclusively for the treatment of

metastatic BC. In metastatic HER2-positive patients, it allows the administration of a higher cumulative dose in combination with trastuzumab and at the same time has less pronounced side effects, such as cardiotoxicity. However, CX did not prove to be more active in resistant cell lines [60]. In addition, combination with DAC did not influence its therapeutic effect, what can be explained by differences in the pharmacokinetics of free and liposomal DOX.

5. Conclusions

Our data indicate enhanced potency of epigenetic inhibitor DAC to reprogram resistant BC cells to standard therapy. Further studies are, however, needed to verify if targeted delivery of epigenetic drugs could improve the efficacy and safety of combination therapy. Despite these encouraging findings, many questions remain open. These include identifying predictive biomarkers, DAC responders vs. non-responders, the role of epigenetic heterogeneity, the limited tolerability, drug administration strategies, sequential vs. concomitant scheduling, functional consequences of lower doses, "one size fits all" approach, or translation of preclinical findings to clinical trials. In addition, the development of new-generation epi-drugs and extensive implementation of omics technologies for patient stratification will allow their broader use in combination with other approaches in the treatment of solid tumors.

CRedit authorship contribution statement

Verona Buocikova: Conceptualization, Investigation, Writing – original draft, Visualization. **Eleonora Marta Longhin:** Investigation, Formal analysis. **Eleftherios Pilalis:** Data curation. **Chara Mastrokalou:** Data curation. **Svetlana Miklikova:** Writing – original draft, Investigation. **Marina Cihova:** Funding Acquisition, Investigation. **Alexandra Poturnayova:** Funding Acquisition, Investigation; **Katarina Mackova:** Investigation. **Andrea Babelova:** Investigation. **Lenka Trnkova:** Investigation. **Naouale El Yamani:** Investigation. **Congying Zheng:** Investigation. **Ivan Rios-Mondragon:** Writing – review & editing. **Martina Labudova:** Investigation. **Lucia Csaderova:** Investigation. **Kristina Mikus Kuracinova:** Investigation. **Peter Makovicky:** Investigation. **Lucia Kucerova:** Supervision. **Miroslava Matuskova:** Investigation, Supervision. **Mihaela Roxana Cimpan:** Funding Acquisition, Writing – review & editing. **Maria Dusinska:** Funding acquisition, Supervision, Writing – review & editing. **Pavel Babal:** Formal analysis, Investigation. **Aristotelis Chatziioannou:** Funding Acquisition, Supervision, Data curation. **Alena Gabelova:** Conceptualization, Writing – original draft. **Elise Rundén-Pran:** Funding Acquisition, Conceptualization, Supervision, Validation, Project administration. **Bozena Smolkova:** Conceptualization, Writing – original draft, Funding acquisition, Project administration, Supervision.

Funding

The following grants supported this research: (7th Joint Translational Call – 2016, European Innovative Research and Technological Development Projects in Nanomedicine) the ERA-NET EuroNanoMed II, project "Innovative Nanopharmaceuticals: Targeting Breast Cancer Stem Cells by a Novel Combination of Epigenetic and Anticancer Drugs with Gene Therapy (ENM II/2016/1121.C/INNOCENT, MIS 5017608)"; Operational Program "Competitiveness, Entrepreneurship and Innovation 2014–2020" (co-funded by the European Regional Development Fund) managed by the Hellenic General Secretariat of Research and Technology, Ministry of Education, Research and Religious Affairs; Research Council of Norway (RCN) projects nos. 271075 (INNOCENT), 288768 (NanoBioReal); APVV-16-0178; APVV-16-0010; ERACo-SysMed/2019/939/RESCUER; Scientific Grant Agency of Slovak Ministry of Education and Slovak Academy of Sciences (VEGA), Grants no. 2/0138/20 and no. 2/0160/21; Research Agency, Grant no.: ITMS

26230120006, and UH-nett Vest. The funding agencies were not involved in the design of the study and collection, analysis, and interpretation of data, and in writing the manuscript.

Declarations

Ethics approval

The animal studies were approved by the Institutional Ethics Committee and by the National Competent Authority of the State Veterinary and Food Administration of the Slovak Republic (Registration Numbers Ro-3616/18-221/3 and Ro-1646/19-221) in compliance with Directive 2010/63/EU of the European Parliament and the European Council and Regulation 377/2012 for the protection of animals used for scientific purposes. All in vivo experiments were performed in the authorized animal facility (license No. SK UCH 02017) in accordance with the Declaration of Helsinki.

Declaration of Competing Interest

The authors declare that they have no known competing financial interests or personal relationships that could have appeared to influence the work reported in this paper.

Availability of data and material

All data generated or analyzed during this study are included in this published article and its supplementary information files.

Acknowledgments

We are grateful to Andrew Collins for his critical reading and English corrections. We would like to thank Marian Grman for his excellent help with the ImageJ software analysis and Lucia Rojikova for her significant contribution to in vivo experiments. Our appreciation also belongs to Alexandra Misci Hudecova, Tatiana Honza, and Erin McFadden for technical assistance and Espen Mariussen for scientific discussions. We would like to thank the Cancer Research Foundation for its continuous help and support. Graphical abstract, Figs. 4, 5, and S5 were created with BioRender.com.

Appendix A. Supporting information

Supplementary data associated with this article can be found in the online version at [doi:10.1016/j.biopha.2022.112662](https://doi.org/10.1016/j.biopha.2022.112662).

References

- R.L. Siegel, K.D. Miller, A. Jemal, Cancer statistics, 2020, *CA Cancer J. Clin.* 70 (1) (2020) 7–30, <https://doi.org/10.3322/caac.21590>.
- C.W.S. Tong, M. Wu, W.C.S. Cho, K.K.W. To, Recent advances in the treatment of breast cancer, *Front. Oncol.* 8 (2018), <https://doi.org/10.3389/fonc.2018.00227> (227–227).
- V. Buocikova, I. Rios-Mondragon, E. Pilalis, A. Chatzizoiannou, S. Miklikova, M. Mego, K. Pajuste, M. Rucins, N.E. Yamani, E.M. Longhin, A. Sobolev, M. Freixanet, V. Puentes, A. Plotniece, M. Dusinska, M.R. Cimpan, A. Gabelova, B. Smolkova, Epigenetics in breast cancer therapy—new strategies and future nanomedicine perspectives, *Cancers* 12 (12) (2020) 3622, <https://doi.org/10.3390/cancers12123622>.
- N.T. Conlon, J.J. Kooijman, S.J.C. van Gerwen, W.R. Mulder, G.J.R. Zaman, I. Diala, L.D. Eli, A.S. Lalani, J. Crown, D.M. Collins, Comparative analysis of drug response and gene profiling of HER2-targeted tyrosine kinase inhibitors, *Br. J. Cancer* 124 (7) (2021) 1249–1259, <https://doi.org/10.1038/s41416-020-01257-x>.
- B. Nami, A. Ghanaeian, C. Black, Z. Wang, Epigenetic silencing of HER2 expression during epithelial-mesenchymal transition leads to trastuzumab resistance in breast cancer, *Life* 11 (9) (2021) 868.
- S. Palomeras, Á. Diaz-Lagares, G. Viñas, F. Setien, H.J. Ferreira, G. Oliveras, A. B. Crujeiras, A. Hernández, D.H. Lum, A.L. Welm, M. Esteller, T. Puig, Epigenetic silencing of TGFBI confers resistance to trastuzumab in human breast cancer, *Breast Cancer Res.* 21 (1) (2019) 79, <https://doi.org/10.1186/s13058-019-1160-x>.
- M. Nava, P. Dutta, R. Farias-Eisner, J.V. Vadgama, Y. Wu, Utilization of NGS technologies to investigate transcriptomic and epigenomic mechanisms in trastuzumab resistance, *Sci. Rep.* 9 (1) (2019) 5141, <https://doi.org/10.1038/s41598-019-41672-6>.
- D. Morel, D. Jeffery, S. Aspeslagh, G. Almouzni, S. Postel-Vinay, Combining epigenetic drugs with other therapies for solid tumours – past lessons and future promise, *Nat. Rev. Clin. Oncol.* 17 (2) (2020) 91–107, <https://doi.org/10.1038/s41571-019-0267-4>.
- M. Kulis, M. Esteller, DNA methylation and cancer, *Adv. Genet.* 70 (2010) 27–56.
- S.R. Bohl, L. Bullinger, F.G. Rücker, Epigenetic therapy: azacytidine and decitabine in acute myeloid leukemia, *Expert Rev. Hematol.* 11 (5) (2018) 361–371, <https://doi.org/10.1080/17474086.2018.1453802>.
- R. Jüttermann, E. Li, R. Jaenisch, Toxicity of 5-aza-2'-deoxycytidine to mammalian cells is mediated primarily by covalent trapping of DNA methyltransferase rather than DNA demethylation, *Proc. Natl. Acad. Sci. USA* 91 (25) (1994) 11797–11801, <https://doi.org/10.1073/pnas.91.25.11797>.
- R.S. Seelan, P. Mukhopadhyay, M.M. Pisano, R.M. Greene, Effects of 5-Aza-2'-deoxycytidine (decitabine) on gene expression, *Drug Metab. Rev.* 50 (2) (2018) 193–207, <https://doi.org/10.1080/03602532.2018.1437446>.
- H.C. Tsai, H. Li, L. Van Neste, Y. Cai, C. Robert, F.V. Rassool, J.J. Shin, K. M. Harbom, R. Beaty, E. Pappou, J. Harris, R.W. Yen, N. Ahuja, M.V. Brock, V. Stearns, D. Feller-Kopman, L.B. Yarmus, Y.C. Lin, A.L. Welm, J.P. Issa, I. Minn, W. Matsui, Y.Y. Jang, S.J. Sharkis, S.B. Baylin, C.A. Zahnow, Transient low doses of DNA-demethylating agents exert durable antitumor effects on hematological and epithelial tumor cells, *Cancer Cell* 21 (3) (2012) 430–446, <https://doi.org/10.1016/j.ccr.2011.12.029>.
- F. Ari, R. Napieralski, E. Ulukaya, E. Dere, C. Colling, K. Honert, A. Krüger, M. Kiechle, M. Schmitt, Modulation of protein expression levels and DNA methylation status of breast cancer metastasis genes by anthracycline-based chemotherapy and the demethylating agent decitabine, *Cell Biochem. Funct.* 29 (8) (2011) 651–659, <https://doi.org/10.1002/cbf.1801>.
- A. Hurtubise, R.L. Momparler, Evaluation of antineoplastic action of 5-aza-2'-deoxycytidine (Dacogen) and docetaxel (Taxotere) on human breast, lung and prostate carcinoma cell lines, *Anticancer Drugs* 15 (2) (2004) 161–167, <https://doi.org/10.1097/00001813-200402000-00010>.
- S. Mirza, G. Sharma, P. Pandya, R. Ralhan, Demethylating agent 5-aza-2-deoxycytidine enhances susceptibility of breast cancer cells to anticancer agents, *Mol. Cell. Biochem.* 342 (1–2) (2010) 101–109, <https://doi.org/10.1007/s11010-010-0473-y>.
- S.Y. Li, R. Sun, H.X. Wang, S. Shen, Y. Liu, X.J. Du, Y.H. Zhu, W. Jun, Combination therapy with epigenetic-targeted and chemotherapeutic drugs delivered by nanoparticles to enhance the chemotherapy response and overcome resistance by breast cancer stem cells, *J. Control Release* 205 (2015) 7–14, <https://doi.org/10.1016/j.jconrel.2014.11.011>.
- B. Pang, X. Qiao, L. Janssen, A. Velds, T. Groothuis, R. Kerkhoven, M. Nieuwland, H. Ovaa, S. Rottenberg, O. van Tellingen, J. Janssen, P. Huijgens, W. Zwart, J. Neefjes, Drug-induced histone eviction from open chromatin contributes to the chemotherapeutic effects of doxorubicin, *Nat. Commun.* 4 (2013), <https://doi.org/10.1038/ncomms2921> (1908–1908).
- G.M. Choong, G.D. Cullen, C.C. O'Sullivan, Evolving standards of care and new challenges in the management of HER2-positive breast cancer, *CA Cancer J. Clin.* 70 (5) (2020) 355–374, <https://doi.org/10.3322/caac.21634>.
- D. Rayson, D. Richel, S. Chia, C. Jackisch, S. van der Vegt, T. Suter, Anthracycline-trastuzumab regimens for HER2/neu-overexpressing breast cancer: current experience and future strategies, *Ann. Oncol.* 19 (9) (2008) 1530–1539, <https://doi.org/10.1093/annonc/mdn292>.
- T.C. Chou, Theoretical basis, experimental design, and computerized simulation of synergism and antagonism in drug combination studies, *Pharmacol. Rev.* 58 (3) (2006) 621–681, <https://doi.org/10.1124/pr.58.3.10>.
- E. Elje, M. Hesler, E. Rundén-Pran, P. Mann, E. Mariussen, S. Wagner, M. Dusinska, Y. Kohl, The comet assay applied to HepG2 liver spheroids, *Mutat. Res.* 845 (2019), 403033, <https://doi.org/10.1016/j.mrgentox.2019.03.006>.
- N. El Yamani, A.R. Collins, E. Rundén-Pran, L.M. Fjellsbø, S. Shaposhnikov, S. Zienoldiny, M. Dusinska, In vitro genotoxicity testing of four reference metal nanomaterials, titanium dioxide, zinc oxide, cerium oxide and silver: towards reliable hazard assessment, *Mutagenesis* 32 (1) (2017) 117–126, <https://doi.org/10.1093/mutage/gew060>.
- A. Dobin, C.A. Davis, F. Schlesinger, J. Drenkow, C. Zaleski, S. Jha, P. Batut, M. Chaisson, T.R. Gingeras, STAR: ultrafast universal RNA-seq aligner, *Bioinformatics* 29 (1) (2013) 15–21, <https://doi.org/10.1093/bioinformatics/bts635>.
- S. Anders, P.T. Pyl, W. Huber, HTSeq—a Python framework to work with high-throughput sequencing data, *Bioinformatics* 31 (2) (2015) 166–169, <https://doi.org/10.1093/bioinformatics/btu638>.
- M.I. Love, W. Huber, S. Anders, Moderated estimation of fold change and dispersion for RNA-seq data with DESeq2, *Genome Biol.* 15 (12) (2014) 550, <https://doi.org/10.1186/s13059-014-0550-8>.
- Y. Tian, T.J. Morris, A.P. Webster, Z. Yang, S. Beck, A. Feber, A.E. Teschendorff, ChAMP: updated methylation analysis pipeline for Illumina BeadChips, *Bioinformatics* 33 (24) (2017) 3982–3984, <https://doi.org/10.1093/bioinformatics/btx513>.
- W.E. Johnson, C. Li, A. Rabinovic, Adjusting batch effects in microarray expression data using empirical Bayes methods, *Biostatistics* 8 (1) (2007) 118–127, <https://doi.org/10.1093/biostatistics/kxj037>.

- [29] A. Akalin, V. Franke, K. Vlahovíček, C.E. Mason, D. Schübeler, Genomation: a toolkit to summarize, annotate and visualize genomic intervals, *Bioinformatics* 31 (7) (2015) 1127–1129, <https://doi.org/10.1093/bioinformatics/btu775>.
- [30] S. Lhomon, T. Avril, N. Dejeans, K. Voutetakis, D. Doultinos, M. McMahon, R. Pineau, J. Obacz, O. Papadodima, F. Jouan, H. Bourien, M. Logotheti, G. Jégou, N. Pallares-Lupon, K. Schmit, P.J. Le Reste, A. Etcheverry, J. Mosser, K. Barroso, E. Vauléon, M. Maurel, A. Samali, J.B. Patterson, O. Pluquet, C. Hetz, V. Quillien, A. Chatziioannou, E. Chevet, Dual IRE1 RNase functions dictate glioblastoma development, *EMBO Mol. Med.* 10 (3) (2018), <https://doi.org/10.15252/emmm.201707929>.
- [31] T. Koutsandreas, I. Binenbaum, E. Pilalis, I. Valavanis, O. Papadodima, A. Chatziioannou, Analyzing and visualizing genomic complexity for the derivation of the emergent molecular networks, *Int. J. Monit. Surveill. Technol. Res. (IJMSTR)* 4 (2) (2016) 30–49.
- [32] The Gene Ontology Consortium, The gene ontology resource: 20 years and still GOing strong, *Nucleic Acids Res.* 47 (D1) (2019) D330–d338, <https://doi.org/10.1093/nar/gky1055>.
- [33] S. Köhler, L. Carmody, N. Vasilevsky, J.O.B. Jacobsen, D. Danis, J.P. Gouridine, M. Gargano, N.L. Harris, N. Matentzoglou, J.A. McMurry, D. Osumi-Sutherland, V. Cipriani, J.P. Balhoff, T. Conlin, H. Blau, G. Baynam, R. Palmer, D. Gratian, H. Dawkins, M. Segal, A.C. Jansen, A. Muaz, W.H. Chang, J. Bergerson, S.J. Lauderdalekind, Z. Yüksel, S. Beltran, A.F. Freeman, P.I. Sergouniotis, D. Durkin, A. L. Storm, M. Hanauer, M. Brudno, S.M. Bello, M. Sincan, K. Rageth, M.T. Wheeler, R. Oegema, H. Loughri, M.G. Della Rocca, R. Thompson, F. Castellanos, J. Priest, C. Cunningham-Rundles, A. Hegde, R.C. Lovering, C. Hajek, A. Olry, L. Notarangelo, M. Similuk, X.A. Zhang, D. Gómez-Andrés, H. Lochmüller, H. Dollfus, S. Rosenzweig, S. Marwaha, A. Rath, K. Sullivan, C. Smith, J.D. Milner, D. Leroux, C.F. Boerkoel, A. Klion, M.C. Carter, T. Groza, D. Smedley, M. A. Haendel, C. Mungall, P.N. Robinson, Expansion of the Human Phenotype Ontology (HPO) knowledge base and resources, *Nucleic Acids Res.* 47 (D1) (2019) D1018–d1027, <https://doi.org/10.1093/nar/gky1105>.
- [34] C.L. Smith, J.T. Eppig, The mammalian phenotype ontology: enabling robust annotation and comparative analysis, *Wiley Inter. Rev. Syst. Biol. Med.* 1 (3) (2009) 390–399, <https://doi.org/10.1002/wsbm.44>.
- [35] B. Jassal, L. Matthews, G. Viteri, C. Gong, P. Lorente, A. Fabregat, K. Sidiropoulos, J. Cook, M. Gillespie, R. Haw, F. Loney, B. May, M. Milacic, K. Rothfels, C. Sevilla, V. Shamovsky, S. Shorsler, T. Varusai, J. Weiser, G. Wu, L. Stein, H. Hermjakob, P. D'Eustachio, The reactome pathway knowledgebase, *Nucleic Acids Res.* 48 (D1) (2020) D498–d503, <https://doi.org/10.1093/nar/gkz1031>.
- [36] K. Moutselos, I. Maglogiannis, A. Chatziioannou, G.Orevenge: a novel generic reverse engineering method for the identification of critical molecular players, through the use of ontologies, *IEEE Trans. Biomed. Eng.* 58 (12) (2011) 3522–3527, <https://doi.org/10.1109/tbme.2011.2164794>.
- [37] D.R. Liston, M. Davis, Clinically relevant concentrations of anticancer drugs: a guide for nonclinical studies, *Clin. Cancer Res.* 23 (14) (2017) 3489–3498, <https://doi.org/10.1158/1078-0432.Ccr-16-3083>.
- [38] P.D. Ottewill, H. Mönkkönen, M. Jones, D.V. Lefley, R.E. Coleman, I. Holen, Antitumor effects of doxorubicin followed by zoledronic acid in a mouse model of breast cancer, *JNCI: J. Natl. Cancer Inst.* 100 (16) (2008) 1167–1178, <https://doi.org/10.1093/jnci/djn240>.
- [39] A.F. Cashen, A.K. Shah, L. Todt, N. Fisher, J. DiPersio, Pharmacokinetics of decitabine administered as a 3-h infusion to patients with acute myeloid leukemia (AML) or myelodysplastic syndrome (MDS), *Cancer Chemother. Pharmacol.* 61 (5) (2008) 759–766, <https://doi.org/10.1007/s00280-007-0531-7>.
- [40] M.W. Pfaffl, G.W. Horgan, L. Dimpfle, Relative expression software tool (REST) for group-wise comparison and statistical analysis of relative expression results in real-time PCR, *Nucleic Acids Res.* 30 (9) (2002), e36, <https://doi.org/10.1093/nar/30.9.e36>.
- [41] M.L. Dahn, B.M. Cruickshank, A.J. Jackson, C. Dean, R.W. Holloway, S.R. Hall, K. M. Coyle, H. Maillet, D.M. Waisman, K.B. Goralski, C.A. Giacomantonio, I.C. G. Weaver, P. Marcato, Decitabine response in breast cancer requires efficient drug processing and is not limited by multidrug resistance, *Mol. Cancer Ther.* 19 (5) (2020) 1110–1122, <https://doi.org/10.1158/1535-7163.Mct-19-0745>.
- [42] T.E. Fandy, A. Jiemjit, M. Thakar, P. Rhoden, L. Suarez, S.D. Gore, Decitabine induces delayed reactive oxygen species (ROS) accumulation in leukemia cells and induces the expression of ROS generating enzymes, *Clin. Cancer Res.: Off. J. Am. Assoc. Cancer Res.* 20 (5) (2014) 1249–1258, <https://doi.org/10.1158/1078-0432.CCR-13-1453>.
- [43] D.Y. Shin, Y.S. Park, K. Yang, G.Y. Kim, W.J. Kim, M.H. Han, H.S. Kang, Y.H. Choi, Decitabine, a DNA methyltransferase inhibitor, induces apoptosis in human leukemia cells through intracellular reactive oxygen species generation, *Int. J. Oncol.* 41 (3) (2012) 910–918, <https://doi.org/10.3892/ijo.2012.1546>.
- [44] Q. Lv, H. Niu, L. Yue, J. Liu, L. Yang, C. Liu, H. Jiang, S. Dong, Z. Shao, L. Xing, H. Wang, Abnormal ferroptosis in myelodysplastic syndrome, *Front. Oncol.* 10 (2020), <https://doi.org/10.3389/fonc.2020.01656> (1656-1656).
- [45] C. Oliveras-Ferraro, B. Corominas-Faja, S. Cuff, A. Vazquez-Martin, B. Martin-Castillo, J.M. Iglesias, E. López-Bonet, G. Martín, Á., J.A. Menendez, Epithelial-to-mesenchymal transition (EMT) confers primary resistance to trastuzumab (Herceptin), *Cell Cycle* 11 (21) (2012) 4020–4032, <https://doi.org/10.4161/cc.22225>.
- [46] Y. Qiu, L. Yang, H. Liu, X. Luo, Cancer stem cell-targeted therapeutic approaches for overcoming trastuzumab resistance in HER2-positive breast cancer, *Stem Cells* 39 (9) (2021) 1125–1136, <https://doi.org/10.1002/stem.3381>.
- [47] K.T. Davidesen, G.S. Haaland, M.K. Lie, J.B. Lorens, A.S. Engelsen, The role of Axl receptor tyrosine kinase in tumor cell plasticity and therapy resistance. *Biomarkers of the Tumor Microenvironment*, Springer, 2017, pp. 351–376.
- [48] X. Gu, R. Tohme, B. Tomlinson, N. Sakre, M. Hasipek, L. Durkin, C. Schuerger, D. Grabowski, A.M. Zidan, T. Radivoyevitch, C. Hong, H. Carraway, B. Hamilton, R. Sobocki, B. Patel, B.K. Jha, E.D. Hsi, J. Maciejewski, Y. Saunthararajah, Decitabine- and 5-azacytidine resistance emerges from adaptive responses of the pyrimidine metabolism network, *Leukemia* 35 (4) (2021) 1023–1036, <https://doi.org/10.1038/s41375-020-1003-x>.
- [49] G.W. Camiener, C.G. Smith, Studies of the enzymatic deamination of cytosine arabinoside. I. Enzyme distribution and species specificity, *Biochem. Pharmacol.* 14 (10) (1965) 1405–1416, [https://doi.org/10.1016/0006-2952\(65\)90175-9](https://doi.org/10.1016/0006-2952(65)90175-9).
- [50] H. Mameri, I. Bièche, D. Meseure, E. Marangoni, G. Buhagiar-Labarchède, A. Nicolas, S. Vacher, R. Onclercq-Delic, V. Rajapakse, S. Varma, Cytidine deaminase deficiency reveals new therapeutic opportunities against cancer, *Clin. Cancer Res.* 23 (8) (2017) 2116–2126.
- [51] S. Noguchi, T. Mori, M. Igase, T. Mizuno, A novel apoptosis-inducing mechanism of 5-aza-2'-deoxycytidine in melanoma cells: demethylation of TNF- α and activation of FOXO1, *Cancer Lett.* 369 (2) (2015) 344–353, <https://doi.org/10.1016/j.canlet.2015.08.023>.
- [52] N.N. Phan, C.Y. Wang, C.F. Chen, Z. Sun, M.D. Lai, Y.C. Lin, Voltage-gated calcium channels: novel targets for cancer therapy, *Oncol. Lett.* 14 (2) (2017) 2059–2074, <https://doi.org/10.3892/ol.2017.6457>.
- [53] G.E. Bertolesi, C. Shi, L. Elbaum, C. Jollimore, G. Rozenberg, S. Barnes, M.E. Kelly, The Ca(2+) channel antagonists mibefradil and pimozide inhibit cell growth via different cytotoxic mechanisms, *Mol. Pharmacol.* 62 (2) (2002) 210–219, <https://doi.org/10.1124/mol.62.2.210>.
- [54] K.K. Wong, DNMT1: a key drug target in triple-negative breast cancer, *Semin. Cancer Biol.* (2020), <https://doi.org/10.1016/j.semcancer.2020.05.010>.
- [55] T. Yokochi, K.D. Robertson, Doxorubicin inhibits DNMT1, resulting in conditional apoptosis, *Mol. Pharmacol.* 66 (6) (2004) 1415–1420, <https://doi.org/10.1124/mol.104.002634>.
- [56] M. Gagliardi, M. Strazzullo, M.R. Matarazzo, DNMT3B functions: novel insights from human disease, *Front. Cell Dev. Biol.* 6 (140) (2018), <https://doi.org/10.3389/fcell.2018.00140>.
- [57] J. Yu, B. Qin, A.M. Moyer, S. Nowsheen, T. Liu, S. Qin, Y. Zhuang, D. Liu, S.W. Lu, K.R. Kalari, D.W. Visscher, J.A. Copland, S.A. McLaughlin, A. Moreno-Aspitia, D. W. Northfelt, R.J. Gray, Z. Lou, V.J. Suman, R. Weinsilboum, J.C. Boughey, M. P. Goetz, L. Wang, DNA methyltransferase expression in triple-negative breast cancer predicts sensitivity to decitabine, *J. Clin. Investig.* 128 (6) (2018) 2376–2388, <https://doi.org/10.1172/JCI97924>.
- [58] L. Simó-Riudalbas, S.A. Melo, M. Esteller, DNMT3B gene amplification predicts resistance to DNA demethylating drugs, *Genes Chromosomes Cancer* 50 (7) (2011) 527–534, <https://doi.org/10.1002/gcc.20877>.
- [59] Y.L. Franco, T.R. Vaidya, S. Ait-Oudhia, Anticancer and cardio-protective effects of liposomal doxorubicin in the treatment of breast cancer, *Breast Cancer* 10 (2018) 131–141, <https://doi.org/10.2147/BCTT.S170239>.
- [60] J. Lao, J. Madani, T. Puértolas, M. Álvarez, A. Hernández, R. Pazo-Cid, Á. Artal, A. Antón Torres, Liposomal doxorubicin in the treatment of breast cancer patients: a review, *J. Drug Deliv.* 2013 (2013), 456409, <https://doi.org/10.1155/2013/456409>.